Combined Valence Bond-Molecular Mechanics Potential Energy Surface and Direct Dynamics Study of Rate Constants and Kinetic Isotope Effects for the H + C$_2$H$_6$ Reaction

Arindam Chakraborty, Yan Zhao, Hai Lin, and Donald G. Truhlar

Department of Chemistry and Supercomputing Institute,

University of Minnesota, Minneapolis, MN 55455-0431

Abstract

This article presents a multi-faceted study of the reaction H + C$_2$H$_6$ $\rightarrow$ H$_2$ + C$_2$H$_5$ and

three of its deuterium-substituted isotopologs. First we present high-level electronic

structure calculations by the W1, G3SX, MCG3-MPWB, CBS-APNO, and MC-QCISD/3

methods that lead to a best estimate of the barrier height of 11.8 ± 0.5 kcal/mol. Then we

obtain a specific reaction parameter for the MPW density functional in order that it

reproduces the best estimate of the barrier height; this yields the MPW54 functional. The

MPW54 functional, as well as the MPW60 functional that was previously parameterized

for the H + CH$_4$ reaction, are used with canonical variational theory with small-curvature

tunneling (CVT/SCT) to calculate the rate constants for all four ethane reactions from

200 to 2000 K. The final MPW54 calculations are based on curvilinear-coordinate

generalized-normal-mode analysis along the reaction-path, and they include scaled

frequencies and an anharmonic C-C bond torsion. They agree with experiment within

31% for 467–826 K except for a 38% deviation at 748 K; the results for the isotopologs

are predictions since these rate constants have never been measured. The kinetic isotope

effects (KIEs) are analyzed to reveal the contributions from subsets of vibrational partition functions and from tunneling, which conspire to yield a nonmonotonic temperature dependence for one of the KIEs. The stationary points and reaction-path potential of the MPW54 potential energy surface are then used to parameterize a new kind of analytical potential energy surface that combines a semiempirical valence bond formalism for the reactive part of the molecule with a standard molecular mechanics force field for the rest; this may be considered to be either an extension of molecular mechanics to treat a reactive potential energy surface or a new kind of combined quantum mechanical/molecular mechanical (QM/MM) method in which the QM part is semiempirical valence bond theory; that is, the new potential energy surface is a combined valence bond molecular mechanics (CVBMM) surface. Rate constants calculated with the CVBMM surface agree with the MPW54 rate constants within 12% for 534–2000 K and within 23% for 200–491 K. The full CVBMM potential energy surface is now available for use in variety of dynamics calculations, and it provides a prototype for developing CVBMM potential energy surfaces for other reactions.

I. INTRODUCTION

One of the ultimate goals of chemistry is to be able to understand and control chemical reaction systems. To realize this goal, one needs to determine the rates of chemical reactions. Thermochemical kinetics is the branch of theoretical chemistry that involves the prediction of the rate constants of chemical reactions by using information about the structures, energies, and vibrational frequencies (or vibrational free energies) of reactants and transition states,[1–3] along with estimates of nonsubstantial contributions[4] (such as tunneling or recrossing) to the free energy of activation. The present article presents an application of thermochemical kinetics to the reaction

$$H + C_2H_6 \rightarrow H_2 + C_2H_5 . \hspace{4cm} (R1)$$

The study of radical–molecule reactions is important in several application areas including combustion, atmospheric chemistry, interstellar chemistry, radiation chemistry, pyrolysis, polymer synthesis, photolysis, oxidation-reduction processes, and aging. The prototype hydrogen transfer reactions of H with CH_4 and C_2H_6 have been studied experimentally (CH_4[5–12] and C_2H_6[5,6,8,12–18]) and theoretically(CH_4[12,19–55]and C_2H_6[12,14,23,56]). Rate constant for $H + CH_4$ has now been calculated quite accurately. In particular it was first shown that variational transition state theory[57,58] with multi-dimensional tunneling contributions[58,59] (VTST/MT) can reproduce quantum mechanical dynamical calculations for a given $H + CH_4$ potential energy surface quite well. Then VTST/MT was applied in direct dynamics calculations with an accurate level of electronic structure theory to predict the rate constant and kinetic isotope effects.

Reaction R1, in contrast, is still remarkably poorly characterized. In 1936, Steacie and Phillips[5] experimentally estimated an activation energy E_a of 6.3 kcal/mol from

measurements at room temperature, and in 1977, Jones *et al.*[16] measured 9.4 kcal/mol in experiments over the temperature range 357–544 K. In 1988, Nicholas and Vaghjiani[18] estimated energy-dependent cross sections from photochemical experiments and thermally averaged them to obtain E_a = 10.8 kcal/mol, which they judged to be "consistent" with the results of Jones *et al.* In 2001, Bryukov *et al.*[14] reported a measurement from 467–826 K that yielded E_a = 8.6 kcal/mol. They could not measure the rate constant at higher temperatures because of dissociation of the radical product. They pointed out that extrapolation to lower and higher temperatures is needed for applications, but the extrapolations are quite ambiguous for a number of reasons. Attempts to extrapolate are uncertain not only because of the uncertainty in E_a but also because of the fact that Arrhenius plots are nonlinear.

Theoretical progress on direct calculations of the rate constant has also been marked by difficulties. In 2001, Senosiain *et al.*[56] modeled the available experimental data and reported an estimated barrier height of 9.7 kcal/mol. Their model also leads to an estimate of the transmission coefficient of 3.6 at 300 K. In contrast, Bryukov *et al.*'s model leads to an estimated barrier height of 9.1 kcal/mol; their rate constant extrapolated to room temperature exceeds the values measured there[5,16,18] by a factor of 3–4. Bryukov *et al.* concluded that "the low-temperature rate constant … remains uncertain."[14] A year later, one of these authors, Knyazev, returned to the problem with a more extensive computational study.[12] Based on isodesmic analyses, he estimated the barrier height at what he considered to be the highest level to be 8.9 kcal/mol (some other calculations[12] gave 9.0 kcal/mol). His extrapolated rate constant at 300 K is 1.2×10^{-17} cm^3 molecules^{-1}s^{-1}, which is a factor of 1.5×10^{-4} lower than the value at

600 K.[12] This compares to 9.4×10^{-17} $cm^3molecules^{-1}s^{-1}$ and a factor of 1.3×10^{-3} in the earlier paper.[14] The difference of an order of magnitude is disconcerting. Kerkeni and Clary[60] used a reduced-dimensionality quantum dynamics method in which two modes are treated in hyperspherical coordinates and the others are modeled using a harmonic approximation. Kerkeni and Clary's potential energy surface has a classical barrier height of 13.5 kcal/mol and a zero-point-inclusive barrier height of 12.0 kcal/mol. In the present study, we will employ full-dimensional VTST/MT to investigate reaction (R1).

As part of the present study a potential energy function (PEF) was constructed for $H + C_2H_6 \rightarrow H_2 + C_2H_5$ by combining semiempirical valence bond theory with molecular mechanics by dividing the entire system into a reactive part and a molecular mechanics (MM) part. This separation was motivated by a similar approach used in QM/MM calculations[61,62] where one divides the system into quantum mechanical part treated by molecular orbital theory and a nonreactive part treated by molecular mechanics; we therefore call the new method the combined valence bond-molecular mechanics (CVBMM) method. For the present application, the VB part is based on the $H + CH_4 \rightarrow H_2 + CH_3$ surface of Joseph et al.[24] and related work by Raff[20] and Jordan et al.,[30] and the MM part uses the standard MM3[63-66] force field. The CVBMM potential energy surface is parameterized against density functional theory (DFT) with a specific reaction parameter (SRP), which in turn is parameterized against a multicoefficient correlation method.

The rate constant calculations were performed by employing variational transition state theory with multidimensional tunneling (VTST/MT), in particular canonical variational theory and the small-curvature tunneling approximation (CVT/SCT). A key

difference between reaction (R1) and the reaction of H with CH_4 is that there is a torsional mode in reaction (R1) that is not present in the H + CH_4 system. The importance of including anharmonicity in the torsion mode for this reaction was emphasized earlier by Senosiain et al.[56] and Sumathi et al.[43] We will therefore pay special attention to the effect of torsional anharmonicity on the calculated reaction rates.

The kinetic isotope effect (KIE) is a ratio of the rates of a chemical reaction when one or more atom in one of the reactants is replaced by one of its isotopes. The study of KIEs is an active area in experimental and theoretical kinetics. Another objective of this study is to predict the rate constants and KIEs for the following reactions using direct dynamics calculations:

$$H + C_2D_6 \rightarrow HD + C_2D_5 \tag{R2}$$

$$D + C_2D_6 \rightarrow D_2 + C_2D_5 \tag{R3}$$

$$D + C_2H_6 \rightarrow DH + C_2H_5 \tag{R4}$$

These KIEs have apparently never been measured.

The analysis of Bryukov et al. was based on conventional transition state theory (TST) calculations without tunneling. Such calculations are inaccurate for two reasons. At low temperature, conventional TST underestimates rate constants due to the fact that it does not include the quantum mechanical tunneling effects. At high temperature, conventional TST tends to overestimate rate constants because of trajectories recrossing a dividing surface through the saddle point at high temperature. The VTST/MT method employed in the present study minimizes the recrossing effect by variationally optimizing the position of the dividing surface in coordinate space, and it also includes multi-dimensional quantum tunneling effects. This represents an improvement over Ref. 60

where only two modes were included in the tunneling dynamics; here 21 modes are included. VTST/MT is the most practical and the most accurate quantum mechanical TST method, and it has been extensively validated.[40,48,67]

In this study, we not only carry out CVT/SCT calculations using CVBMM, we also carry out CVT/SCT calculations by direct dynamics. In the direct dynamics method,[25,40,59,68–72] all potential energy surface (PES) information for each geometry is obtained from electronic structure calculations directly (without using a fit). In other words, the PES is implicitly defined by an electronic structure level that is used to provide energies, gradients, and Hessians to the dynamics calculations on the fly. We also use a specific-reaction-parameter (SRP) approach[73] for the PES. The SRP method we used is called MPWX.[74] It is a one-parameter hybrid density functional method.

The details of the CVBMM functional form of the potential energy surface are given in Sec. II. Section III presents the CVT/SCT method that will be used for dynamics calculations. The high-level electronic structure methods used to estimate the barrier height and the DFT-SRP methods used to parameterize the CVBMM potential energy surface are provided in Sec. IV. Section V provided the details of the software used for the calculations. In Secs. VI and VII we present the results and discussion. Section VIII contains concluding remarks.

II. CVBMM POTENTIAL ENERGY SURFACE

In the CVBMM method, the potential energy V of the entire system is expressed as the sum of the potential energy V_{VB} of the reactive part, the potential energy V_{MM} of the molecular mechanics part, and the VB/MM interaction term:

$$V = V_{\text{VB}} + V_{\text{MM}} + V_{\text{VB/MM}}. \qquad (1)$$

We will illustrate the method for reaction (R1), but it can be applied to a diverse range of reactions. Although potential energy surfaces based on valence bond theory are available for many small-molecule reactions,[75–77] the method becomes unwieldy for larger molecules.[78,79] CVBMM method allows one to combine convenient valence bond functional forms for a small reactive fragment with standard molecular mechanics[80,81] potentials for the nonreactive parts of the reactants in order to obtain analytical potential energy functions suitable for calculating reactive dynamics.

For the $H + C_2H_6$ reaction, the reactive part consists of the attacking hydrogen atom labeled as H_9 in Fig. 1, the carbon atom (labeled as C_1) from which hydrogen is abstracted, and the three hydrogen atoms (labeled as H_6, H_7 and H_8) centered on this carbon. The MM part consists of the methyl group (labeled as C_2, H_3, H_4, H_5) that is bonded to the reactive carbon atom. The molecular mechanics term is calculated using the MM3 force field.[63–66] The functional forms of the VB/MM interactions terms are constructed by introducing switching functions in the functional forms of the MM3 force field. A subset of parameters is changed from their original values in the V_{VB} and the $V_{\text{VB/MM}}$ functional forms to adjust the energy of reaction, the barrier height, the geometries, and the corresponding frequencies of reactant, products, and saddle point against the DFT calculation described in Sec. IV. The functional forms of the reactive and molecular mechanics terms are described in the rest of Sec. II, and the parameterization is discussed in Sec. VII.

II.A. Molecular Mechanical Terms

Molecular mechanics interactions are generally expressed in valence internal coordinates[82] such as bond lengths, bond angles, and torsional angles, and the potential energy is expressed in terms of bond stretching, angle bending, torsion, Coulomb, and van der Waals interactions. In the CVBMM method, in order to decide which interactions should be treated using MM, we use the same criterion that has been used successfully for other QM/MM calculations;[83] in particular, all interactions that involve at least one MM atom are treated using molecular mechanics terms. One of the limitations of molecular mechanics force fields is their inability to handle atoms and bonds that change their character as the reaction progresses. All molecular mechanics interactions that change their character during course of the reaction, i.e., appear or disappear, are treated as VB/MM interactions terms, whereas terms that retain that form (with or without geometry-dependent parameters) maybe in either V_{MM} or $V_{VB/MM}$. In general, any interaction involving at least one MM and one VB atom is included in the $V_{VB/MM}$ term, and all interactions that do not involve any VB atom are treated using the molecular mechanics and are included in the V_{MM} term.

The MM3 force field[63–66] is used in the present paper to calculate all the molecular mechanics interactions. The details of MM3 are given in Ref. 63–66, and the equations relevant to the present work are summarized in the supporting information.[84]

In general V_{MM} contains the MM terms for which all atoms in the MM subsystem. For, the present reaction, V_{MM} contains three C-H stretches, three H-C-H bending terms, and stretch-bend and bend-bend cross terms. In general, an MM force field would also include Coulomb terms, but in the present example, the MM subsystem

is a hydrocarbon fragment, and MM3 does not include Coulomb interactions for hydrocarbons. The relevant MM3 expressions used in the present paper are summarized in the supporting information.[84]

II.B. VB/MM Interaction

Due to the difference in the bonding (i.e., connectivity pattern) between the reactant and products, there are some interactions that are present in the reactant but are absent in the product. According to the prescription that we include all MM interactions that involve at least one MM atom, $V_{VB/MM}$ contains the following interactions in either reactant or product: C-C stretch, H-C-C bend, H-C-C-H torsion, stretch-bend interactions, bend-bend interactions, stretch-torsion cross terms, and van der Waals interactions. To make the discussion concrete, we consider the abstraction of H_8 by H_9 in Fig. 1. The C-C-H bend term between H_8, C_1, and C_2 is present in ethane but absent in the ethyl radical since the C_1-H_8 bond is broken during the course of the reaction. The three H-C-C-H torsion terms associated with the H_8 hydrogen atom are other examples of interactions that are present in the reactant but absent in the product. The reactant and the product both include interaction of H_3, H_4, and H_5 with H_6, H_7, and H_8. Note that, as an additional simplification in the present work, all van der Waals interactions involving H_9 are not included.

In addition to interactions that appear or disappear as the reaction proceeds, other interactions are present all along the reaction-path but with different parameters in reactants and products. For example, the equilibrium C-C distances for the reactant, saddle point, and the product obtained from the DFT calculations are 1.51, 1.50, and 1.48

Å, respectively. To extend the force field to treat such interactions, we have introduced

two geometry-dependent switching functions T_1 and T_2. The first of these is defined as:

$$T_1(r_{C_1H_i}) = 0.5(1 - \tanh[w_1(r_{C_1H_i} - w_2)]), \tag{2}$$

where w_1 and w_2 are adjustable parameters. Two MM3 parameters, one bend term, and

three torsion terms are modulated by T_1. The reference C-C bond distance parameter and

the reference C-C-H bond angle parameter are transformed smoothly from reactant to

product using the equations

$$r^0_{CC, VB/MM} = P_1 r^0_{CC,R} + (1 - P_1) r^0_{CC,P}, \tag{3}$$

$$\theta^0_{CCH, VB/MM} = P_1 \theta^0_{CCH,R} + (1 - P_1) \theta^0_{CCH,P}, \tag{4}$$

where,

$$P_1 = \prod_{i=6}^{8} T_1(r_{C_1H_i}). \tag{5}$$

Note that P_1 in the above equation is symmetric with respect to all the three hydrogen

atoms and goes to zero as one of the hydrogen atoms is abstracted. To emphasize the fact

that the reference bond distance and bond angle are not constants (as they are in the MM3

force field) but depend on geometry, they are labeled as $r^0_{CC, VB/MM}$ and $\theta^0_{CCH, VB/MM}$,

respectively. To annihilate the valence interactions that are present in the reactant (R) but

are absent in the products (P), the corresponding MM3 terms are multiplied by the T_1

switching function.

The T_2 switching function is given by

$$T_2(\rho) = 0.5(1 - \tanh[w_3(\rho - w_4)]), \tag{6}$$

where w_3 and w_4 are adjustable parameters and ρ is a unitless quantity defined as

$$\rho = \frac{(r_{C_1H_6} + r_{C_1H_7} + r_{C_1H_8})}{3}(\frac{1}{r_{H_9H_6}} + \frac{1}{r_{H_9H_7}} + \frac{1}{r_{H_9H_8}}). \qquad (7)$$

The corresponding geometry dependent force constants are denoted by $k_{CC,\,VB/MM}$ and $k_{CCH,\,VB/MM}$, respectively, and are transformed using the T_2 switching function

$$k_{CC,\,VB/MM} = T_2 k_{CC,R} + (1 - T_2)k_{CC,P}, \qquad (8)$$

$$k_{CCH,\,VB/MM} = T_2 k_{CCH,R}^{\theta} + (1 - T_2)k_{CCH,P}^{\theta}. \qquad (9)$$

In the supporting information,[84] a term-by-term description is provided for all terms used in the evaluation of the $V_{VB/MM}$ energy.

II.C. Reactive Part

The reactive part of the system is modeled using semiempirical valence bond theory. In particular, we modified the functional for the $H + CH_4 \rightarrow H_2 + CH_3$ potential energy surface by Joseph $et\ al.$[24] and Jordan $et\ al.$[30] which are based on older work by Raff.[20] These older functions are in turn based on functional forms based on the valence bond treatment of London.[75] Recently,[46] the parameters in the Jordan $et\ al.$ surface were modified to give better agreement with the experimental results. Since construction of the CVBMM surface also involves reoptimization of the parameters in the Jordan $et\ al.$ surface, the surface described in Ref. 46 was not used in the present work. The functional form of the CH_4 surface was defined by Jordan $et\ al.$[30] in terms of C-H bond vectors. In the present work we used similar bond vectors that are defined as follows. The vectors $\mathbf{u}_1, \mathbf{u}_2$, and $\mathbf{u}_3$ are the three bond vectors along the C_1-H_6, C_1-H_7, and C_1-H_8 bonds,

respectively. The bond vector $\mathbf{u}_4$ is defined as scaled C-C bond vector and was obtained

by multiplying the bond vector along the C_1-C_2 bond by the factor α_{scale}. The value of

α_{scale} was obtained from the ratio of the C-C and C-H equilibrium bond distances in

ethane. This yields $\alpha_{\text{scale}} = 0.717$. This treatment is identical to the scaling of C-C bonds

in QM/MM calculations using a hydrogen link atom.[83] The magnitudes of the four

vectors $(\mathbf{u}_i, i = 1, \ldots, 4)$ are denoted as $(u_i, i = 1, \ldots, 4)$.

To express the functional forms in a compact notation, the H_6-H_9, H_7-H_9, and H_8-

H_9 internuclear distances are called $r_{\text{HH},1}, r_{\text{HH},2}$ and $r_{\text{HH},3}$, respectively. The V_{VB} energy

is written as a sum of stretch (str), out-of-plane bending (op), and in-plane bending (ip)

terms

$$V_{\text{VB}} = \sum_{i=1}^{3} V_{\text{JG}}^{\text{str}}(u_i, r_{\text{C}_1\text{H}_9}, r_{\text{HH},i})\zeta(\rho) + V_{\text{JG}}^{\text{op}} + V_{\text{JG}}^{\text{ip}}, \tag{10}$$

where $V_{\text{JG}}^{\text{str}}$ is a three-body LEPS function.[24] The expressions[20,24,30] for $V_{\text{JG}}^{\text{str}}$, $V_{\text{JG}}^{\text{op}}$, and

$V_{\text{JG}}^{\text{ip}}$, presented in the supporting information.[84]

Note that each LEPS term involves three different kinds of interaction: C_1-H_i

interactions with $i = 6, 7, 8$; H_i-H_9 interaction with $i = 6, 7, 8$; and C_1-H_9 interaction. The H_9

hydrogen atom does not form a bond with the C_1 carbon atom, and different Morse

parameters were used by Joseph $et\ al.$[22] and Jordan $et\ al.$[30] for C_1-H_9, and C_1-H_i

($i = 6,7,8$) interactions. The sets of Morse parameters for C_1-H_9, C_1-H_i, and H_i-H_9

interactions are labeled as $({}^1D_{\text{C}_1\text{H}_9}, {}^3D_{\text{C}_1\text{H}_9}, \alpha_{\text{C}_1\text{H}_9}, r^0_{\text{C}_1\text{H}_9})$, $({}^1D_{\text{CH}}, {}^3D_{\text{CH}}, \alpha_{\text{CH}}, u^0)$

and $({}^1D_{\text{HH}}, {}^3D_{\text{HH}}, \alpha_{\text{HH}}, r^0_{\text{HH}})$, respectively. In the present functional form, the Morse

parameters u^0, r_{HH}^0, and $^1D_{HH}$ were smoothly changed from reactant (R) to product (P)

as follows:

$$u^0 = (1 - T_3)u_R^0 + T_3 u_P^0, \tag{11}$$

$$r_{HH}^0 = (1 - T_3)r_{HH,R}^0 + T_3 r_{HH,P}^0, \tag{12}$$

$$^1D_{HH} = (1 - T_3)^1D_{HH,R} + T_3 {}^1D_{HH,P}, \tag{13}$$

where the switching function is defined as

$$T_3 = 0.5(1 - \tanh[w_5(\bar{u} - \bar{u}^0)]), \tag{14}$$

with w_5 as an adjustable parameter and

$$\bar{u} = \frac{1}{3}\sum_{i=1}^{3} u_i. \tag{15}$$

The term $\zeta(\rho)$ in Eq. (10) was not present in the original CH_4 surface and is a new

modification for the present surface to provide more flexibility. It has the following form

$$\zeta(\rho) = \sum_{i=1}^{6} \lambda_i g_i(\chi, d_i, \rho), \tag{16}$$

$$g_i(\chi, d_i, \rho) = e^{-\chi(\rho - d_i)^2}, \tag{17}$$

where χ, λ_i, and d_i are adjustable parameters.

III. VARIATIONAL TRANSITION STATE THEORY

III.A. Reaction-Path Potentials and Rate Constants

Detailed accounts of variational transition state theory (VTST) are given

elsewhere.[57,58,85–89] Here we summarize the key quantities used in the calculations.

Canonical variational theory (CVT) is the version of VTST in which the transition state is

optimized for a canonical ensemble. The CVT method as applied here minimizes the

calculated rate constant at a given temperature as a function of the distance s along the

reaction-path of sequence of dividing hypersurfaces (generalized transition states or

GTSs) transverse to the minimum energy path (MEP) through an isoinertial coordinate

system. The potential along the MEP is called $V_{\text{MEP}}(s)$, and adding the local zero point

energy to this yields the vibrationally adiabatic ground-state potential energy curve,

$V_a^G(s)$. The value of $V_{\text{MEP}}(s)$ at the saddle point, relative to reactants, is called $V_f^{\neq}$ and

relative to products is called $V_r^{\neq}$. The value of $V_a^G(s)$ at the saddle point, relative to

reactants, is called $\Delta V_a^{G\neq}$. The value of $V_a^G(s)$ at products minus that at reactants is

ΔH_0.

The CVT rate constant including multidimensional tunneling contributions used

for the present study is

$$k^{\text{CVT/SCT}} = \kappa^{\text{SCT}}(T)k^{\text{CVT}}(T), \tag{18}$$

where κ^{CVT} is the rate constant calculated by CVT (as explained in more detail in the

supporting information[84]), and κ^{SCT} is the transmission coefficient used to include

quantum effects on reaction coordinate motion, where the superscript stands for the small

curvature tunneling (SCT) approximation.[59,89]

III.B. Hindered Rotator Approximation

In the $H + C_2H_6$ system, there is a vibrational mode corresponding to the torsional

motion around the C-C bond. We treat this torsional mode by using a hindered rotator

(HR) approximation scheme that was developed earlier.[90] In this HR treatment, the

partition functions for the torsion are calculated by interpolation between the limits for

harmonic oscillators and for free internal rotators. We use the RW scheme proposed in a

previous paper,[72] and we note that we showed recently that this RW scheme can give

reasonable estimates of the ^{13}C KIEs for the OH + CH$_4$ reaction.[91] The internal rotation

barrier W is calculated by a torsional scan with the MPW54 method. This yields

$W = 2.75$ kcal/mol for the reactant, and the value of W for the transition state is given in

Sec. VI.D.

IV. ELECTRONIC STRUCTURE THEORY

IV.A. High-Level Methods

To obtain the energetics of reaction (R1), we performed several calculations using

wave function theory (WFT), in particular we carried out G3SX,[92] MCG3-MPWB,[93] MC-

QCISD/3,[94] W1,[95] and CBS-APNO[96] calculations to calculate the classical barrier height

and energy of reaction. The results of these WFT calculations are compared to results

calculated by density functional theory (DFT) in Tables I–IV. (The CVBMM results in

Tables I, II, and IV will be explained in Sec. VII.)

IV.B. DFT

Another electronic structure method that we used in the present study is density

functional theory. The DFT calculations are based on a hybrid Fock-Kohn-Sham operator,

which can be written as follows[97, 98]

$$F = F^{\text{H}} + (X/100)F^{\text{HFE}} + (1 - X/100)(F^{\text{SE}} + F^{\text{GCE}}) + F^{\text{C}}, \qquad (19)$$

where F^{H} is the Hartree operator (i.e., the nonexchange part of the Hartree-Fock

operator), F^{HFE} is the Hartree-Fock exchange operator, X is the percentage of Hartree-Fock exchange, F^{SE} is Slater's local density functional for exchange, F^{GCE} is the gradient correction for the exchange functional, and F^C is the correlation functional. When a modified Perdew-Wang (mPW) functional[99] is employed with 25% Hartree-Fock exchange ($X = 25$) and the Perdew-Wang correlation functional (PW91),[100] this is MPW1PW91 in GAUSSIAN03.[101] Using the 6-31+G(d, p) basis set, Lynch and Truhlar[42,97] parameterized Eq. (19) with these choices of functionals against a database of barrier heights and energies of reactions. The resulting 1-parameter method is called modified Perdew-Wang (MPW) functional for kinetics is (MPW1K), in which $X = 42.8$. Pu and Truhlar[45,48] also parameterized Eq. (19) with these functionals for the H + CH$_4$ reaction, yielding MPW60 for which $X = 60$. The latter is called a specific reaction parameter (SRP)[59,73] approach because the parameter is optimized for one reaction. In the next section we reoptimize X for reaction (R1).

IV.C. Parameterization of the DFT-SRP Functional

A general scheme to improve the accuracy of the one-parameter DFT surfaces for a specific reaction is to vary the percentage of HF exchange so that the predicted surface provides a better representation for the specific reaction of interest. Recently we[102] have shown that the 6-31+G(d,p)[103] basis set can provide useful accuracy for energies of reaction and reaction barrier height with DFT methods. Thus, we used 6-31+G(d,p) basis set with the MPWX for reaction (R1). (In general, MPWX denotes the functional obtained as in the previous subsection but for a given percentage X of Hartree-Fock exchange.) We adjust the value of X in Eq. (19) so that the MPWX method yields an energy of reaction

equal to experimental value, –0.43 kcal/mol, for the reaction (R1). (This experimental energy of reaction is obtained from the MGAE109/05[93,94] database of zero-point-exclusive experimental atomization energies.) This yields a new DFT-SRP functional, MPW54, that has 54% Hartree-Fock exchange.

V. SOFTWARE

The W1 calculations were carried out with the MOLPRO program.[104] The G3SX and MCG3-MPWB calculations were performed with the MLGAUSS[105] program in conjunction with the GAUSSIAN03[101] program. The calculation of $k^{CVT/SCT}$ reported below were performed using GAUSSRATE[106] which interfaces the VTST/MT program POLYRATE[107] to the electronic structure program GAUSSIAN03.[101] The GAUSSRATE, MLGAUSS, and POLYRATE programs can be downloaded from the Truhlar group's software webpage.[108] The CVBMM potential energy surface is available in POTLIB.[109,110]

VI. RESULTS FROM DIRECT DYNAMICS CALCULATIONS

VI.A. Details of the Calculations

In the dynamics calculations, the scaling mass for all coordinates is set equal to 1 amu. The minimum energy path (MEP) in the isoinertial coordinate system is followed by the Page-McIver algorithm.[111] The gradient step size is 0.005 a_0 and the Hessian is calculated every 9 steps. We scaled all DFT vibrational frequencies along the reaction coordinate, and we used 0.9415 as the scaling factor for the MPW54/6-31+G(d,p) method and 0.9312 for MPW60/6-31+G(d,p). These scaling factors were optimized against the ZPE13/99 database,[112] which is a database of thirteen anharmonic vibrational zero point

energies (ZPEs). The coordinate system for the generalized normal mode analysis along the reaction-path is a set of redundant curvilinear internal coordinates.[113]

VI.B. Energetics

Table I is the summary of the energetics calculated by different methods. The barrier heights calculated by the G3SX, CBS-APNO, MC-QCISD/3, W1, MCG3-MPWB, and MPWX methods are in good agreement with one another, but they are lower than the barrier height from Kerkeni and Clary's CCSD(T)/cc-pVTZ //MP2/cc-pVTZ calculation by about 2 kcal/mol. Rate constants that are calculated with the PES based on the CCSD(T)/cc-pVTZ calculations by Kerkeni and Clary are therefore much lower than the experimental rate constant. This is an indication that Kerkeni and Clary's[60] CCSD(T)/cc-pVTZ calculation overestimates the barrier height of the reaction (R1). The barrier height obtained by the MPW60/6-31+G(d,p) method of Pu and Truhlar[40] is close to the W1 calculation. The HDFT-SRP method developed in this study, MPW54/6-31+G(d,p), gives a similar barrier height to that from the MCG3-MPWB method. Table II lists the zero point energies, vibrationally adiabatic ground-state barrier height, and enthalpy of reaction. Table III gives a comparison of the calculated forward ($V_f^{\neq}$) and reverse ($V_r^{\neq}$) barrier heights for H + CH$_4$ and H + C$_2$H$_6$ reactions using various[92–96] high-level methods. Table III shows that G3SX, CBS-APNO, W1, and MCG3-MPWB give similar barrier heights and a similar trend in the difference between the two reactions, but the CCSD(T,full) method without extrapolation is unreliable.

VI.C. Transition State Geometries and Imaginary Frequencies

Table IV gives the key geometric parameters of the transition state, which include the length of the breaking-bond (C-H) and that of the forming-bond (H-H) in the transition state of H + C_2H_6, and their sum is also included in the table; this quantity is called perpendicular looseness, and it measures the looseness of the transition state structure in a direction perpendicular to the reaction coordinate.[42] In our previous work, the MC-QCISD/3 method has proved to be able to provide accurate geometries for stable molecules[114] and for transition states.[112]

From Table IV, we can see that MC-QCISD/3 gives a very similar transition state geometry to that obtained by the QCISD/6-311++G(2df,2p) method. If we use the MC-QCISD/3 geometry as a reference, the MP2/cc-pVTZ method gives a shorter H-H bond (forming-bond) and a longer C-H bond (breaking-bond), whereas MPW54 and MPW60 give more accurate transition state geometries.

VI.D. Torsional Potential

The lowest-frequency mode of the reactant is an internal rotation. Figure 2 presents the torsional potential for the transition state of reaction (R1) at the MPW54/6-31+G(d,p) level of theory. The barrier associated with this internal rotation is 707 cm^{-1} (2.02 kcal/mol). We used this barrier for all generalized transition states in the HR calculations in POLYRATE.

VI.E. Barrier Shape

Figure 3 presents the adiabatic ground-state potential curve, $V_a^G(s)$ for reactions

(R1)–(R4). The shoulders in Fig. 3 result from competition between a decreasing potential energy and an increasing zero-point contribution. The Born-Oppenheimer potential along the MEP for reactions (R1)–(R4) is provided in the supporting information.[84]

VI.F. Reaction Rate Constants

Reaction rate constants obtained from dynamical calculations and corresponding experimental values for the H + C_2H_6 reaction are given in Table V. We compared three different dynamics calculations, in particular, calculations based on MPW60/6-31+G(d,p) and MPW54/6-31+G(d,p) surfaces with the harmonic approximation and one based on the MPW54/6-31+G(d,p) surface with hindered rotator anharmonicity. To analyze the variational and tunneling effects, we list rate constants for conventional transition state theory (TST), for canonical variational transition state theory (CVT), and for CVT with multi-dimensional tunneling contributions calculated in the small-curvature tunneling approximation (CVT/SCT).

If we compare the CVT/SCT harmonic rate constants at 637 K, we see that rate constant from the MPW60 surface with the harmonic approximation underestimates the rate constant by 28%, and that from the MPW54 surface overestimates it by 10%. The HR approximation lowers the CVT/SCT rate constant, and the rate constant from the MPW54 surface with the HR approximation agrees well with experiment. More broadly the mean absolute deviation from experiment at the eleven temperatures from 467 to 826 K is only 15%, and the mean deviation is only +4%. These deviations are within the experimental uncertainty. The maximum deviation from experiment is 38% at 748 K, and

the second largest deviation is 31% at 826 K.

The difference between the TST and CVT values is a measure of how much recrossing occurs at the conventional transition state and can be recovered by variational optimization of the transition state. For the MPW54(HR) calculation, Table V shows that variational optimization of the transition state location reduces the rate constant for H transfer by 22% at 200 K, 7–14% at 300–491 K, and 6% or less for 534–2000 K. The net effect of the tunneling and nonclassical reflection contributions increases the CVT rate constant by factors of 370, 12, and 3.8 at 200, 300, and 400 K, respectively, by 65% at 637 K, by 22% at 1000 K, and by 5% at 2000 K.

The rate constants calculated by using conventional TST with one-dimensional Wigner tunneling (TST/W) for the MPW54/6-31+G(d,p) surface are given in the supporting information.[84]

VI.G. Kinetic Isotope Effects

The KIE is defined as the ratio k_i / k_j where k_i is the rate constant for the isotopic reaction with lighter mass, and k_j is the rate constant for the corresponding heavier isotopic reaction. KIEs greater than 1 are called "normal," and those less than 1 are called "inverse". Table VI lists the rate constants for reactions (R2)–(R4), and Figures 4–6 are the plots of temperature dependences of KIEs. Figures 4 and 5 show that the KIEs for H + C_2H_6/H + C_2D_6 and H + C_2H_6/D + C_2D_6 are normal and monotonically decreasing with increasing temperature. Figure 6 shows that H + C_2H_6/D + C_2H_6 shows an inverse KIE.

The CVT/SCT KIE for H + C_2H_6/D + C_2H_6 shows a nonmonotonic temperature

dependence. At high temperature, the KIE increases with increasing temperature, whereas at low temperature, it decreases with increasing temperature. To explain this phenomenon, we performed a factorization analysis for the KIEs of $H + C_2H_6/D + C_2H_6$. The factors are listed in Table VII, which shows that the CVT KIE is monotonically increasing (with increasing temperature) due to $\eta_{vib,mid}$. From an analysis of the contributions to $\eta_{vib,mid}$ from each of the modes, we found that the main contribution is from the quasi-symmetric stretch mode of the forming-bond and breaking-bond. Table VII also shows that the tunneling contribution, η_{tun}, tends to increase the KIEs at low temperatures. The interplay of $\eta_{vib,mid}$ and η_{tun} produces the nonmonotonic temperature dependence.

VII. PARAMETERIZATION OF THE CVBMM POTENTIAL ENERGY SURFACE

Geometry dependence in the reference C-C bond distance and the reference C-C-H bond angle is introduced by using Eq. (3) and (4). The force constants for the C-C stretch and C-C-H bend are varied as shown in Eqs. (8) and (9), respectively. The parameters $w_1,\ldots,w_5$ are optimized to give the correct frequencies and geometry at the saddle point. The parameters w_1 and w_2 control the rate of switching of the T_1 and T_2 switching functions. It was found that using a fast switching rate for the force constants would introduce a spurious shoulder near the saddle point in the ground-state adiabatic potential energy curve, and therefore the force constants were switched more slowly than the bond distances to avoid this. One of the major differences between the $H + CH_4$ and

the H + C_2H_6 reactions is the exothermicity of the two reactions. The methane reaction is endothermic while the ethane reaction is exothermic. The $^1D_{HH}$ Morse parameter in the product region is optimized to get the correct exothermicity. The reference bond distances of Eqs. (11) and (12) are also changed as the reaction progresses from reactants to products. The scaling function $\zeta(\rho)$ in Eq. (10) was obtained by least squares calculation minimizing the root mean square (RMS) deviation in energies along the minimum energy path obtained using MPW54/6-31+G(d,p) . This was crucial to get the correct shape and the width of the barrier. All other parameters are fixed at the literature values.[30] The parameters used in the CVBMM surface are given in the supporting information.[84]

VII.A. Energetics and Geometries

The geometries of the reactant, products, and the saddle point are in good agreement with the MPW54/6-31+G(d,p) calculations. Table VIII lists the optimized geometries of reactant, products, and the saddle point obtained from the CVBMM potential energy surface. The energy of reaction and the barrier height obtained from the CVBMM potential energy surface are in good agreement with the MPW54/6-31+G(d,p) calculations as shown in Table I. The torsional barrier height in the CVBMM potential energy surface is found to be 2.14 kcal/mol and is in good agreement with MPW54 value (higher by only 0.12 kcal/mol).

VII.B. Frequencies

Table IX lists the vibrational frequencies of the reactant, products, and the saddle point obtained at the optimized geometries from the CVBMM potential energy surface.

The mean signed error (MSE) and the mean unsigned error (MUE) in the frequencies of the bound vibrational modes between scaled MPW54/6-31+G(d,p) and the CVBMM surface are 2 and 50 cm^{-1} for ethane, -27 and 49 cm^{-1} for ethyl radical, and -2 and 68 cm^{-1} for saddle point geometries. The frequency in the CVBMM surface associated with the unbound mode at the saddle point is 176 cm^{-1} higher than the MPW54 value.

VII.C. Barrier Shape and Rate Constants

The V_{MEP} and V_a^G curves obtained from the CVBMM surface are shown in Figs. 7 and 8, respectively; they are in good agreement with the MPW54 calculations. Note that the generalized normal mode frequencies along the minimum energy path for the CVBMM surface are in good agreement with MPW54 calculations and are responsible for giving good agreement in the V_a^G curves. In the dynamics calculations, the scaling mass for all coordinates is set equal to 1 amu. The MEP is followed by the Page-McIver algorithm[111] with a gradient step size is 0.005 a_0. Since the CVBMM surface is optimized against the scaled MPW54/6-31+G(d,p) frequencies, a frequency-scale factor of 1.0 is used for the rate constant calculations. The reaction rate constants calculated using the CVBMM surface are listed in Table X along with the MPW54/6-31+G(d,p) results. The average percent deviation of the CVBMM rate constants from the MPW54/6-31+G(d,p) ones is calculated using the formula:

$$\text{Average \% deviation} = \frac{1}{18} \sum_{i=1}^{18} \left| \frac{k^{CVBMM} - k^{MPW54}}{k^{MPW54}} \right| \times 100 , \qquad (20)$$

and the values for TST, CVT, and CVT/SCT are 31, 29, and 33 %, respectively.

The rate constants calculated by using conventional TST with one-dimensional

Wigner tunneling (TST/W) for the CVBMM surface are given in the supporting

information.[84]

VIII. CONCLUDING REMARKS

In this work, we developed an analytical CVBMM surface for the H + C_2H_6

abstraction reaction. We performed variational transition state theory calculations with

multidimensional tunneling to calculate rate constants and KIEs using both direct

dynamics and the new CVBMM potential energy surface. The CVBMM method provides

a systematic procedure for classifying vibrational interactions and is a general method for

fitting analytical potential energy surfaces that can be applied to larger systems. For

example, applying the CVBMM method to H + C_3H_8 or H + C_4H_{10} would involve an

increase in the number of valence terms in MM energy and the number of van der Waals

interactions in the VB/MM energy, but would not require new parameters or more

expensive quantum mechanical (semiempirical VB) calculations, although one may have

to reoptimize the set of parameters used in defining the switching functions to reproduce

the desired geometry and frequencies at the saddle point. The desired values for the

exothermicity, barrier height, and shape of the barrier can be achieved by optimizing a

small number of parameters in the VB term.

We investigated the effect of anharmonicity by using the HR approximation. The

calculated rate constants agree well with experimental results. The KIE for H + C_2H_6/D +

C_2H_6 shows different temperature dependences in different temperature regions due to

the interplay of the contributions from the vibrational partition function and the

contributions from tunneling.

Finally, we provide a few remarks to place this work in context. The CVBMM method may be considered to be a special case of the combined quantum mechanical and molecular mechanical (QM/MM) method, which has been reviewed elsewhere.[117–122] The various combined QM/MM methods are distinguished by the choice of QM treatment and by the way that the QM and MM subsystems are joined together. For example, the QM method may be semiempirical molecular orbital theory,[123–133] ab initio wave function theory[83,124,134–141] (WFT), or density functional theory[83,124,142–148] (DFT). Here, following Raff[20] and Joseph *et al.*,[24] we use semiempirical valence bond theory for the QM part. As far as joining the QM and MM parts, the present treatment is very similar to the way QM is joined to MM in previous work.[83,124,136] The advantage of CVBMM over previous combined QM/MM methods is that the potential evaluations are very rapid, and one can obtain very precise and inexpensive analytical gradients and Hessians for classical dynamics. The disadvantage is that semiempirical valence bond theory has less predictive value than high-level WFT or DFT. However this limitation can be overcome by fitting the parameters to higher-level calculations, as is done in the example $H + C_2H_6$ presented in this article.

ACKNOWLEDGMENT

REFRENCES

[1] D. R. Herschbach, H. S. Johnston, K. S. Pitzer, and R. E. Powell, J. Chem. Phys. **25**, 736 (1956).

[2] H. S. Johnston, Adv. Chem. Phys. **3**, 131 (1960).

[3] S. W. Benson, in *Thermochemical Kinetics*, 2nd ed. (John Wiley & Sons, New York, 1976).

[4] D. G. Truhlar and B. C. Garrett, J. Am. Chem. Soc. **111**, 1232 (1989).

[5] E. W. R. Steacie and N. W. F. Phillips, J. Chem. Phys. **4**, 461 (1936).

[6] R. Wolfgang, Acc. Chem. Res. **2**, 248 (1969).

[7] W. E. Jones and J. L. Ma, Can. J. Chem. **64**, 2192 (1986).

[8] D. L. Baulch, C. J. Cobos, R. A. Cox, C. Esser, P. Frank, T. Just, J. A. Kerr, M. J. Pilling, J. Troe, R. W. Walker, and J. Warnatz, J. Phys. Chem. Ref. Data, **21**, 411 (1992).

[9] V. D. Knyazev, A. Bencsura, S. I. Stoliarov, and I. R. Slagle, J. Phys. Chem. **100**, 11346 (1996).

[10] M. G. Bryukov, I. R. Slagle, and V. D. Knyazev, J. Phys. Chem. A **105**, 3107 (2001).

[11] J. W. Sutherland, M.-C. Su, and J. V. Michael, Int. J. Chem. Kinet. **33**, 669 (2001).

[12] V. D. Knyazev, J. Phys. Chem. A **106**, 11603 (2002).

[13] G. J. Germann, Y.-D. Huh, and J. J. Valentini, J. Chem. Phys. **96**, 5746, (1992).

[14] M. G. Bryukov, I. R. Slagle, and V. D. Knyazev, J. Phys. Chem. A **105**, 6900 (2001).

[15] V. V. Azatyan and S. B. Filippov, Dokl. Phys. Chem. **184**, 49 (1969).

[16] D. Jones, P. A. Morgan, and J. H. Purnell, J. Chem. Soc. Faraday Trans. I **73**, 1311 (1977).

[17] J. Lede and J. Villermaux, Can. J. Chem. **56**, 392 (1978).

[18]J. E. Nicholas and G. L. Vaghjiani, J. Chem. Phys. **89**, 3388 (1988).

[19]K. Morokuma and R. E. Davis, J. Am. Chem. Soc. **94**, 1060 (1972).

[20]L. M. Raff, J. Chem. Phys. **60**, 2220 (1974).

[21]G. C. Schatz, S. P. Walch, and A. F. Wagner, J. Chem. Phys. **73**, 4536 (1980).

[22]G. C. Schatz, A. F. Wagner, and J. T. H. Dunning, J. Phys. Chem. **88**, 221 (1984).

[23]D. G. Truhlar, R. Steckler, and M. S. Gordon, Chem. Rev. **87**, 217 (1987).

[24]T. Joseph, R. Steckler, and D. G. Truhlar, J. Chem. Phys. **87**, 7036 (1987).

[25]K. K. Baldridge, M. S. Gordon, R. Steckler, and D. G. Truhlar, J. Phys. Chem. **93**, 5107 (1989).

[26]G. A. Natanson, B. C. Garrett, T. N. Truong, T. Joseph, and D. G. Truhlar, J. Chem. Phys. **94**, 7875 (1991).

[27]E. Kraka, J. Gauss, and D. Cremer, J. Chem. Phys. **99**, 5306 (1993).

[28]D. Dobbs and D. A. Dixon, J. Phys. Chem. **98**, 5290 (1994).

[29]T. N. Truong and W. Duncan, J. Chem. Phys. **101**, 7408 (1994).

[30]M. J. T. Jordan and R. G. Gilbert, J. Chem. Phys. **102**, 5669 (1995).

[31]T. Takayanagi, J. Chem. Phys. **104**, 2237 (1996).

[32]T. Taketsugu and M. J. Gordon, J. Chem. Phys. **104**, 2834 (1996).

[33]J. Espinosa-Garcia and J. C. Corchado, J. Phys. Chem. **100**, 16561 (1996).

[34]Z. Konkli, E. Kraka, and D. Cremer, J. Phys. Chem. A **101**, 1742 (1997).

[35]T. Takata, T. Taketsugu, K. Hirao, and M. S. Gordon, J. Chem. Phys. **109**, 4281 (1998).

[36]Y. Kurosaki and T. Takayanagi, Chem. Phys. Lett. **299**, 57 (1999).

[37]H.-G. Yu and G. Nyman, J. Chem. Phys. **111**, 3508 (1999).

[38]A. Fernández-Ramos, E. Martínez-Núñez, Z. Smedarchina, and S. A. Vázquez, Chem.

Phys. Lett. **341**, 351 (2001).

[39]D. Y. Wang and J. M. Bowman, J. Chem. Phys. **115**, 2055 (2001).

[40]J. Pu, J. C. Corchado, and D. G. Truhlar, J. Chem. Phys. **115**, 6266 (2001).

[41]H.-G. Yu and G. Nyman, J. Phys. Chem. A **105**, 2240 (2001).

[42]B. J. Lynch and D. G. Truhlar, J. Phys. Chem. A **105**, 2936 (2001).

[43]R. Sumathi, H.-H. Carstensen, and J. W. H. Green, J. Phys. Chem. A **105**, 6910 (2001).

[44]G. D. Billing, Chem. Phys. **277**, 325 (2002).

[45]J. Pu and D. G. Truhlar, J. Chem. Phys. **116**, 1468 (2002).

[46]J. Espinosa-Garcia, J. Chem. Phys. **116**, 10664 (2002).

[47]J. Palma, J. Echave, and D. C. Clary, J. Phys. Chem. A **106**, 8256 (2002).

[48]J. Pu and D. G. Truhlar, J. Chem. Phys. **117**, 1479 (2002).

[49]M. L. Wang and J. Z. H. Zhang, J. Chem. Phys. **117**, 3081 (2002).

[50]H. Szichman and R. Baer, J. Chem. Phys. **117**, 7614 (2002).

[51]J. Pu and D. G. Truhlar, J. Chem. Phys. **117**, 10675 (2002).

[52]X. Zhang, G. H. Yang, K. L. Han, M. L. Wang, and J. Z. H. Zhang, J. Chem. Phys. **118**, 9266 (2003).

[53]Y. Zhao, B. J. Lynch, and D. G. Truhlar, J. Phys. Chem. A **108**, 2715 (2004).

[54]Y. Zhao, T. Yamamoto, and W. H. Miller, J. Chem. Phys. **120**, 3100 (2004).

[55]T. Wu, H. J. Werner, and V. Manthe, Science **306**, 2227 (2004).

[56]J. P. Senosiain, C. B. Musgrave, and D. M. Golden, J. Phys. Chem. A **105**, 1669 (2001).

[57]B. C. Garrett and D. G. Truhlar, J. Phys. Chem. **83**, 1079 (1979).

[58]D. G. Truhlar, A. D. Isaacson, and B. C. Garrett, in *Theory of Chemical Reaction Dynamics*, edited by M. Baer (CRC Press, Boca Raton, 1985), Vol. 4, p. 65.

[59]Y.-P. Liu, G. C. Lynch, T. N. Truong, D.-H. Lu, D. G. Truhlar, and B. C. Garrett, J. Am. Chem. Soc. **115**, 2408 (1993).

[60]B. Kerkeni and D. C. Clary, J. Chem. Phys. **121**, 6809 (2004).

[61]*Combined Quantum Mechanical and Molecular Mechanical Methods*, edited by J. Gao and M. A. Thompson (American Chemical Society, Washington, 1998).

[62]J. Gao and D. G. Truhlar, Annu. Rev. Phys. Chem. **53**, 467 (2002).

[63]N. L. Allinger, J. Am. Chem. Soc. **99**, 8551 (1977).

[64]N. L. Allinger, Y. H. Yuh, and J.-H. Lii, J. Am. Chem. Soc. **111**, 8127 (1989).

[65]J.-H. Lii and N. L. Allinger, J. Am. Chem. Soc. **111**, 8567 (1989).

[66]J.-H. Lii and N. L. Allinger, J. Am. Chem. Soc. **111**, 8576 (1989).

[67]T. C. Allison and D. G. Truhlar, in *Modern Methods for Multidimensional Dynamics Computations in Chemistry*, edited by D. L. Thompson (World Scientific, Singapore, 1998), p. 618.

[68] I. S. Y. Wang and M. Karplus, J. Am. Chem. Soc. **95**, 8160 (1973).

[69]D. J. Malcome-Lawes, J. Chem. Soc. Faraday Trans. II **71**, 1183 (1973).

[70]C. Leforestier, J. Chem. Phys. **68**, 4406 (1978).

[71]E. Uggerud and T. Helgakar, J. Am. Chem. Soc. **114**, 4265 (1992).

[72]Y.-Y. Chuang and D. G. Truhlar, J. Chem. Phys. **112**, 1221 (2000).

[73]A. Gonzalez-Lafont, T. N. Truong, and D. G. Truhlar, J. Phys. Chem. **95**, 4618 (1991).

[74]P. Winget, J. D. Thompson, J. D. Xidos, C. J. Cramer, and D. G. Truhlar, J. Phys. Chem. A **106**, 10707 (2002).

[75]C. A. Parr and D. G. Truhlar, J. Phys. Chem. **75**, 1844 (1971).

[76]D. G. Truhlar, R. Steckler, and M. S. Gordon, Chem. Rev. **87**, 217 (1987).

[77]G. C. Schatz, Rev. Mod. Phys. **61**, 669 (1989).

[78]H. Eyring and G. E. Kimball, J. Chem. Phys. **1**, 239 (1933).

[79]M. B. Faist and J. T. Muckerman, J. Chem. Phys. **71**, 225 (1979).

[80]J. P. Bowen and N. L. Allinger, Rev. Comp. Chem. **2**, 81 (1991).

[81]A. R. Leach, *Molecular Modeling*, 2nd ed. (Prentice-Hall, Harlow, 2001).

[82]E. B. Wilson, J. C. Decius, and P. C. Cross, *Molecular Vibrations* (Dover, New York, 1980).

[83]H. Lin and D. G. Truhlar, J. Phys. Chem. A **109**, 3991 (2005).

[84]See EPAPS Document No.___ for a brief description of canonical variational theory, factorization analysis of the KIEs, functional forms of relevant MM3 equations, list of MM3 parameters, rate constants calculated by the TST/W method using MPW54/6-31+G(d,p), and CVBMM potential energy surface. A direct link to this document may be found in the online article's HTML reference section. The document may also be reached via EPAPS homepage (http://www.aip.org/pubservs/epaps.html) or from ftp.aip.org in the directory /epaps. See the EPAPS homepage for more information.

[85]B. C. Garrett, D. G. Truhlar, R. S. Grev, and A. W. Magnuson, J. Phys. Chem. **84**, 1730 (1980).

[86]D. G. Truhlar and B. C. Garrett, Annu. Rev. Phys. Chem. **35**, 159 (1984).

[87]S. C. Tucker and D. G. Truhlar, in *New Theoretical Concepts for Understanding Organic Reactions*, edited by J. Bertran and I. G. Csizmadia (Kluwer, Dordrecht, 1989), Vol. 267, p. 291.

[88]B. C. Garrett and D. G. Truhlar, in *Encyclopedia of Computational Chemistry*, edited by P. v. R. Schleyer, N. L. Allinger, T. Clark, J. Gasteiger, P. A. Kollman, H. F. Schaefer

III, and P. R. Schreiner (John Wiley & Sons, Chichester, 1998), Vol. 5, p. 3094.

[89]D.-h. Lu, T. N. Troung, V. S. Melissas, G. C. Lynch, Y.-P. Liu, B. C. Garrett, R. Steckler, A. D. Isaacson, S. N. Rai, G. C. Hancock, J. G. Lauderdale, T. Joseph, and D. G. Truhlar, Comput. Phys. Commun. **71**, 235 (1992).

[90]D. G. Truhlar, J. Comp. Chem. **12**, 266 (1991).

[91]H. Lin, Y. Zhao, B. A. Ellingson, J. Pu, and D. G. Truhlar, J. Am. Chem. Soc. **127**, 2830 (2005).

[92]L. A. Curtiss, P. C. Redfern, K. Raghavachari, and J. A. Pople, J. Chem. Phys. **114**, 108 (2001).

[93]Y. Zhao, B. J. Lynch, and D. G. Truhlar, Phys. Chem. Chem. Phys. **7**, 43 (2005).

[94]B. J. Lynch and D. G. Truhlar, J. Phys. Chem. A **107**, 3898 (2003).

[95]J. M. L. Martin and G. D. Oliveira, J. Chem. Phys. **111**, 1843 (1999).

[96]J. W. Ochterski, G. A. Petersson, and J. A. Montgomery Jr., J. Chem. Phys. **104**, 2598 (1996).

[97]B. J. Lynch, P. L. Fast, M. Harris, and D. G. Truhlar, J. Phys. Chem. A **104**, 4811 (2000).

[98]A. D. Becke, J. Chem. Phys. **104**, 1040 (1996).

[99]C. Adamo and V. Barone, J. Comp. Chem. **19**, 419 (1998).

[100]K. Burke, J. P. Perdew, and Y. Wang, in *Electronic Density Functional Theory: Recent Progress and New Directions*, edited by J. F. Dobson, G. Vignale, and M. P. Das (Plenum, New York, 1998), p. 81.

[102]M. J. Frisch, G. W. Trucks, H. B. Schlegel, G. E. Scuseria, M. A. Robb, J. R. Cheeseman, J. A. Montgomery, Jr., T. Vreven, K. N. Kudin, J. C. Burant, J. M. Millam, S. S. Iyengar, J. Tomasi, V. Barone, B. Mennucci, M. Cossi, G. Scalmani, N. Rega, G.

A. Petersson, H. Nakatsuji, M. Hada, M. Ehara, K. Toyota, R. Fukuda, J. Hasegawa, M. Ishida, T. Nakajima, Y. Honda, O. Kitao, H. Nakai, M. Klene, X. Li, J. E. Knox, H. P. Hratchian, J. B. Cross, C. Adamo, J. Jaramillo, R. Gomperts, R. E. Stratmann, O. Yazyev, A. J. Austin, R. Cammi, C. Pomelli, J. W. Ochterski, P. Y. Ayala, K. Morokuma, G. A. Voth, P. Salvador, J. J. Dannenberg, G. Zakrzewski, S. Dapprich, A. D. Daniels, M. C. Strain, O. Farkas, D. K. Malick, A. D. Rabuck, K. Raghavachari, J. B. Foresman, J. V. Ortiz, Q. Cui, A. G. Baboul, S. Clifford, J. Cioslowski, B. B. Stefanov, G. Liu, A. Liashenko, P. Piskorz, I. Komaromi, R. L. Martin, D. J. Fox, T. Keith, M. A. Al-Laham, C. Y. Peng, A. Nanayakkara, M. Challacombe, P. M. W. Gill, B. Johnson, W. Chen, M. W. Wong, C. Gonzalez, and J. A. Pople. GAUSSIAN 03; Revision C.01; Gaussian, Inc.: Pittsburgh PA, 2003.

[102]B. J. Lynch, Y. Zhao, and D. G. Truhlar, J. Phys. Chem. A **107**, 1384 (2003).

[103]R. Krishnan, J. S. Binkley, R. Seeger, and J. A. Pople, J. Chem. Phys. **72**, 650 (1980).

[104]H.-J. Werner, P. J. Knowles, R. D. Amos, A. Bernhardsson, A. Berning, P. Celani, D. L. Cooper, M. J. O. Deegan, A. J. Dobbyn, F. Eckert, C. Hampel, G. Hetzer, T. Korona, R. Lindh, A. W. Lloyd, S. J. McNicholas, F. R. Manby, W. Meyer, M. E. Mura, A. Nicklass, P. Palmieri, R. Pitzer, G. Rauhut, M. Schütz, U. Schumann, H. Stoll, A. J. Stone, R. Tarroni, and T. Thorsteinsson. MOLPRO–2002.6; University of Birmingham: Birmingham, 2002.

[105]Y. Zhao and D. G. Truhlar. MLGAUSS–version 1.0; University of Minnesota: Minneapolis, 2004.

[106]J. C. Corchado, Y.-Y. Chuang, E. L. Coitiño, and D. G. Truhlar. GAUSSRATE–9.0; 9.0/P9.0-G94/G98; University of Minnesota: Minneapolis, May 2002.

[107]J. C. Corchado, Y.-Y. Chuang, P. L. Fast, J. Villa, W.-P. Hu, Y.-P. Liu, G. C. Lynch, K. A. Nguyen, C. F. Jackels, V. S. Melissas, B. J. Lynch, I. Rossi, E. L. Coitiño, A. Fernandez-Ramos, J. Pu, T. V. Albu, R. Steckler, B. C. Garrett, A. D. Isaacson, and D. G. Truhlar. POLYRATE– 9.1; University of Minnesota: Minneapolis, 2002.

[108]D. G. Truhlar. http://comp.chem.umn.edu/mccdir/software.htm.

[109]R. J. Duchovic, Y. L. Volobuev, G. C. Lynch, D. G. Truhlar, T. C. Allison, A. F. Wagner, B. C. Garrett, and J. C. Corchado, Comp. Phys. Commun. **144**, 169 (2002), **156**, 319(E) (2004).

[110]R. J. Duchovic, Y. L. Volobuev, G. C. Lynch, A. W. Jasper, D. G. Truhlar, T. C. Allison, A. F. Wagner, B. C. Garrett, J. Espinosa-García, and J. C. Corchado. POTLIB-online, http://comp.chem.umn.edu/potlib

[111]M. Page and J. W. McIver, J. Chem. Phys. **88**, 922 (1988).

[112]Y. Zhao, B. J. Lynch, and D. G. Truhlar, J. Phys. Chem. A **108**, 4786 (2004).

[113]K. A. Nguyen, C. F. Jackels, and D. G. Truhlar, J. Chem. Phys. **104**, 6491 (1996).

[114]J. M. Rodgers, P. L. Fast, and D. G. Truhlar, J. Chem. Phys. **112**, 3141 (2000).

[115]A. D. Bosese and J. M. L. Martin, J. Chem. Phys. **121**, 3405 (2004).

[116]B. Kerkeni and D. C. Clary, J. Chem. Phys. **120**, 2308 (2004).

[117]J. Gao, Rev. Comp. Chem. **7**, 119 (1996).

[118]P. Sherwood, in *Modern Methods and Algorithms of Quantum Chemistry*, edited by J. Grotenhaus (Neumann Institute for Computing, Jülich, 2000), p. 285.

[119]J. Gao and D. G. Truhlar, Annu. Rev. Phys. Chem. **53**, 467 (2002).

[120]A. Shurki and A. Warshel, Adv. Protein Chem. **66**, 249 (2003).

[121]R. A. Friesner and V. Guallar, Annu. Rev. Phys. Chem. **56**, 389 (2005).

[122]H. Lin and D. G. Truhlar, Theor. Chem. Acc., to be published.

[123]M. J. Field, P. A. Bash, and M. Karplus, J. Comput. Chem. **11**, 700 (1990).

[124]P. D. Lyne, M. Hodoscek, and M. Karplus, J. Phys. Chem. A **103**, 3462 (1999).

[125]J. J.Ruiz-Pernia, E. Silla, I. Tunon, S. Marti, and V. Moliner, J. Phys. Chem. B **108**, 8427 (2004).

[126]J. Pu, J. Gao, and D. G. Truhlar, J. Phys. Chem. A **108**, 5454 (2004).

[127]P. M. Gleeson, I. H. Hillier, and N. A. Burton, Org. Biomol. Chem. **2**, 2275 (2004).

[128]H. Park, E. N. Brothers, and K. M. Merz, Jr. J. Am. Chem. Soc. **127**, 4232 (2004).

[129]P. L. Cummins and J. E. Gready, J. Comp. Chem. **26**, 561 (2005).

[130]B. A. Gregersen, J. Khandogin, W. Thiel, and D. M. York, J. Phys. Chem. B **109**, 9810 (2005).

[131]S. Ferrer, J. J. Ruiz-Pernia, I. Tuñon, V. Moliner, M. Garcia-Viloca, A. Gonzalez-Lafont, and J. M. Lluch, J. Chem. Theory Comp. **1**, 750 (2005).

[132]O. Acevedo and W. L. Jorgensen, J. Am. Chem. Soc. **127**, 8829 (2005).

[133]H. Hu and W. Yang, J. Chem. Phys. **123**, 41102 (2005).

[134]M. Freindorf and J. Gao, J. Comp. Chem. **17**, 386 (1996).

[135]X. Assfeld and J.-L. Rivail, Chem. Phys. Lett. **263**, 100 (1996).

[136]J. Pu, J. Gao, and D. G. Truhlar, J. Phys. Chem. A **108**, 632 (2004).

[137]D. Xu, H. Guo, J. Gao, and Q. Cui, Chem. Comm. **7**, 892 (2004).

[138]A. Osted, J. Kongsted, K. V. Mikkelsen, and O. Christiansen, J. Phys. Chem. A **108**, 8646 (2004).

[139]J. H. Jensen, H. Li, A. D. Robertson, and P. A. Molina, J. Phys. Chem. A **109**, 6634 (2005).

[140]M. Klaehn, S. Braun-Sand, E. Rosta, and A. Warshel, J. Phys. Chem. B **109**, 15645 (2005).

[141]Q. M. Fatmi, T. S. Hofer, B. R. Randolf, and B. M. Rode, J. Chem. Phys. **123**, 054514 (2005).

[142]I. Tuñon, M. T. C. Martins-Costa, C. Millot, and M. F. Ruiz-Lopez, J. Chem. Phys. **106**, 3633 (1997).

[143]P. M. Dal, L. I. Llarrull, U. Rothlisberger, A. J. Vila, and P. Carloni, J. Am. Chem. Soc. **126**, 12661 (2004).

[144]J.-W. Chu, B. R. Brooks, and B. L. Trout, J. Am. Chem. Soc. **126**, 16601 (2004).

[145]M. Hoffmann, I. V. Khavrutskii, D. G. Musaev, and K. Morokuma, Int. J. Quant. Chem. **99**, 972 (2004).

[146]A. A. Sokol, S. T. Bromley, S. A. French, C. Catlow, A. Richard, and P. Sherwood, Int. J. Quant. Chem. **99**, 695 (2004).

[147]G. Drudis-Sole, G. Ujaque, F. Maseras, and A. Lledos, Chem. Eur. J. **11**, 1017 (2005).

[148]H. M. Senn, D. O'Hagan, and W. Thiel, J. Am. Chem. Soc. **127**, 13643 (2005).

[149]J. Pu, J. Gao, and D. G. Truhlar, ChemPhysChem **6**, 1853 (2005).

Table I. Energetics for the reaction $H + C_2H_6$ (kcal/mol).[a]

Method	$V_f^{\neq}$	ΔE	$V_r^{\neq}$
WFT			
G3SX[b]	12.21	−0.52	12.73
CBS-APNO[b]	11.54	−0.48	12.02
CBS-APNO[c]	11.55	−0.49	12.04
MC-QCISD/3[b]	12.33	−1.22	13.55
W1[b]	12.02	−0.55	12.57
W1[c]	12.05	−0.55	12.60
CCSD(T, full)/cc-pVTZ[d]	13.50	4.10	9.40
WFT/DFT			
MCG3-MPWB[b]	11.44	−0.99	12.43
MCG3-MPWB[c]	11.42	−0.99	12.41
DFT			
MPW54/6-31+G(d,p)	11.45	−0.43	11.88
MPW60/6-31+G(d,p)	11.98	−0.32	12.30
Analytic			
CVBMM	11.45	−0.43	11.88
Experiment[e]	–	−0.43	–

[a]$V_f^{\neq}$ is the forward classical barrier height, $V_r^{\neq}$ is the reverse classical barrier height, and ΔE is the classical energy of reaction.

[b]MC-QCISD/3 geometries are used.

[c]MPWB1K/MG3S geometries are used.

[d]MP2/cc-pVTZ geometries are used. These calculations are from Ref. 60

[e]Reference 102

Table II. ZPEs, differences in ZPE between saddle point and reactants and between saddle point and products, ground-state

vibrationally adiabatic barrier height at the saddle point, and enthalpy of reaction (kcal/mol) at 0 K.

Method	ZPE						Energetics	
	C_2H_6	C_2H_5	H_2	S.P.	S.P.–R	S.P.–P	$\Delta V_a^{G^{\neq}}$	ΔH_0
WFT								
MC-QCISD/3	46.55	37.10	6.20	44.81	−1.74	1.50	10.59	−4.47
CCSD(T,full)/cc-pVTZ[a]	47.75	38.65	6.47	46.22	−1.53	1.09	12.00	1.50
DFT								
MPW54/6-31+G(d,p)	45.82	36.44	6.15	44.22	−1.60	1.63	9.85	−3.65
MPW60/6-31+G(d,p)	45.64	36.30	6.12	44.02	−1.61	1.61	10.37	−3.54
Analytic								
CVBMM	45.78	36.87	6.38	44.27	−1.50	1.03	9.95	−2.96

[a]MP2/cc-pVTZ geometries are used.

Table III. Comparison of calculated barrier heights (kcal/mol) for $H + CH_4 \rightarrow H_2 + CH_3$ and $H + C_2H_6 \rightarrow H_2 + C_2H_5$ reactions.

Method	CH$_4$		C$_2$H$_6$		Difference	
	$V_f^{\ddagger}$	$V_r^{\ddagger}$	$V_f^{\ddagger}$	$V_r^{\ddagger}$	$\Delta V_f^{\ddagger}$	$\Delta V_r^{\ddagger}$
WFT						
G3SX[a]	15.15	12.23	12.21	12.73	2.94	−0.50
CBS-APNO[a]	14.67	11.30	11.54	12.02	3.13	−0.72
MC-QCISD/3[a]	15.13	12.88	12.33	13.55	2.81	−0.67
W1[a,b]	14.88	11.89	12.02	12.57	2.86	−0.68
CCSD(T, full)/cc-pVTZ[c]	15.48	11.78	13.50	9.40	1.98	2.38
DFT						
MPW54/DIDZ[d]	14.34	10.86	11.45	11.88	2.89	−1.02
MPW60/DIDZ[d]	14.80	11.10	11.98	12.30	2.82	−1.20
WFT/DFT						
MCG3-MPWB[a]	14.46	11.62	11.44	12.43	3.02	−0.80

[a]For the G3SX, CBS-APNO, MC-QCISD/3, W1, MCG3-MPWB calculations, the QCISD/MG3 geometries are used for the H + CH$_4$ reaction, and MC-QCISD/3 geometries are used for the H + C$_2$H$_6$ reaction. Note that the QCISD/MG3 geometries are very close to the MC-QCISD/3 ones.

[b]The W1 results for the H + CH$_4$ are taken from Ref. 115.

[c]The MP2(full)/cc-pVTZ geometries are used for the CCSD(T, full)/cc-pVTZ calculation and the results are taken from. Refs. 60 and 116.

[d]For the MPW54 and MPW60 DFT methods, the consistently optimized geometries are used for each level of theory.

Table IV. Geometries and imaginary frequencies for the saddle point.[a]

Method	Bond lengths			Bond angle		Imaginary
	H-H	C-H	Sum	$\angle$C-H-H	$\angle$H-C-C-H	frequency
WFT						
MP2(full)/cc-pVTZ[b]	0.866	1.417	2.283	178	180	1498i
QCISD/6-311++G(2df,2p)	0.925	1.355	2.280	177	180	-
MC-QCISD/3	0.924	1.354	2.278	176	180	1474i
DFT						
MPW54/6-31+G(d,p)	0.912	1.355	2.267	178	180	1359i
MPW60/6-31+G(d,p)	0.912	1.353	2.265	177	180	1392i
WFT/DFT						
MCG3-MPWB[a]	0.924	1.354	2.278	176	180	1474i
Analytic						
CVBMM	0.922	1.355	2.277	179	180	1537i

[a]Distances are in Å, bond angles are in degrees, and frequencies are in cm^{-1}.

[b]Reference 60.

Table V. Direct dynamics rate constants (cm^3 molecule^{-1} s^{-1}) for the H + C$_2$H$_6$ reaction.[a]

T (K)	MPW60 (HO)			MPW54 (HO)			MPW54 (HR)			Experiment
	TST	CVT	CVT/SCT	TST	CVT	CVT/SCT	TST	CVT	CVT/SCT	
200	4.76E-22	4.00E-22	1.78E-19	1.77E-21	1.44E-21	5.29E-19	1.66E-21	1.29E-21	4.77E-19	n.a.
300	3.05E-18	2.77E-18	3.20E-17	7.29E-18	6.50E-18	7.62E-17	6.87E-18	5.90E-18	6.96E-17	n.a.
400	2.68E-16	2.53E-16	9.16E-16	5.14E-16	4.80E-16	1.81E-15	4.84E-16	4.37E-16	1.66E-15	n.a.
467	1.92E-15	1.85E-15	4.61E-15	3.36E-15	3.20E-15	8.28E-15	3.15E-15	2.91E-15	7.61E-15	1.04E-14
491	3.45E-15	3.33E-15	7.55E-15	5.86E-15	5.60E-15	1.32E-14	5.49E-15	5.10E-15	1.21E-14	1.42E-14
534	8.69E-15	8.43E-15	1.67E-14	1.41E-14	1.36E-14	2.78E-14	1.32E-14	1.24E-14	2.56E-14	2.86E-14
586	2.25E-14	2.20E-14	3.84E-14	3.50E-14	3.40E-14	6.10E-14	3.26E-14	3.09E-14	5.61E-14	5.45E-14
600	2.82E-14	2.75E-14	4.69E-14	4.35E-14	4.26E-14	7.36E-14	3.97E-14	3.86E-14	6.79E-14	n.a.
612	3.42E-14	3.35E-14	5.58E-14	5.22E-14	5.09E-14	8.67E-14	4.85E-14	4.62E-14	7.96E-14	7.88E-14
637	4.98E-14	4.89E-14	7.80E-14	7.47E-14	7.30E-14	1.19E-13	6.93E-14	6.61E-14	1.09E-13	1.08E-13
693	1.06E-13	1.04E-13	1.54E-13	1.53E-13	1.50E-13	2.26E-13	1.41E-13	1.36E-13	2.07E-13	2.21E-13
748	2.00E-13	1.98E-13	2.76E-13	2.82E-13	2.78E-13	3.92E-13	2.59E-13	2.50E-13	3.58E-13	2.59E-13
776	2.69E-13	2.67E-13	3.62E-13	3.74E-13	3.70E-13	5.07E-13	3.43E-13	3.32E-13	4.62E-13	4.40E-13
796	3.29E-13	3.26E-13	4.36E-13	4.53E-13	4.48E-13	6.04E-13	4.15E-13	4.02E-13	5.50E-13	4.45E-13
826	4.36E-13	4.33E-13	5.67E-13	5.95E-13	5.88E-13	7.74E-13	5.42E-13	5.27E-13	7.04E-13	5.36E-13
1000	1.69E-12	1.68E-12	2.01E-12	2.17E-12	2.16E-12	2.58E-12	1.95E-12	1.90E-12	2.31E-12	n.a.
1500	1.75E-11	1.75E-11	1.86E-11	2.06E-11	2.06E-11	2.20E-11	1.75E-11	1.75E-11	1.86E-11	n.a.
2000	6.62E-11	6.62E-11	6.80E-11	7.45E-11	7.45E-11	7.66E-11	6.03E-11	5.96E-11	6.23E-11	n.a.

[a]The 6-31+G(d,p) basis set used. HO denotes the harmonic oscillator approximation for all modes; HR denotes that the lowest-frequency mode is treated as a hindered rotator.

Table VI. Direct dynamics rate constants (cm^3 molecule^{-1} s^{-1}) for the H + C_2D_6, D + C_2D_6, and D +C_2H_6 reactions.[a]

T (K)	H + C_2D_6			D + C_2D_6			D + C_2H_6		
	TST	CVT	CVT/SCT	TST	CVT	CVT/SCT	TST	CVT	CVT/SCT
200	6.48E-23	5.00E-23	2.61E-21	3.06E-22	2.88E-22	1.13E-20	7.92E-21	7.59E-21	6.93E-19
300	7.85E-19	6.73E-19	2.70E-18	1.90E-18	1.84E-18	7.53E-18	1.71E-17	1.66E-17	1.26E-16
400	9.60E-17	8.68E-17	1.78E-16	1.70E-16	1.67E-16	3.51E-16	8.85E-16	8.70E-16	2.74E-15
491	1.49E-15	1.38E-15	2.18E-15	2.25E-15	2.22E-15	3.58E-15	8.57E-15	8.46E-15	1.82E-14
600	1.46E-14	1.40E-14	1.85E-14	1.92E-14	1.90-E14	2.61E-14	5.62E-14	5.57E-14	9.27E-14
612	1.72E-14	1.64E-14	2.17E-14	2.29E-14	2.27E-14	3.07E-14	6.69E-14	6.63E-14	1.08E-13
748	1.12E-13	1.08E-13	1.29E-13	1.37E-13	1.36E-13	1.66E-13	3.29E-13	3.27E-13	4.55E-13
1000	1.03E-12	1.01E-12	1.11E-12	1.16E-12	1.16E-12	1.29E-12	2.28E-12	2.27E-12	2.73E-12
1500	1.11E-11	1.11E-11	1.13E-11	1.17E-11	1.17E-11	1.22E-11	1.84E-11	1.84E-11	1.99E-11
2000	4.04E-11	4.01E-11	4.08E-11	4.21E-11	4.21E-11	4.31E-11	6.50E-11	6.47E-11	6.78E-11

[a]All calculations in this table use the MPW54/6-31+G(d,p) electronic structure level and use the HR approximation for the lowest-frequency mode.

Table VII. KIEs and factors for the $H + C_2H_6/D + C_2H_6$.[a]

T (K)	η_{trans}	η_{rot}	η_{vib}				η_{pot}	η^{CVT}[b]	η_{tun}	$\eta^{CVT/SCT}$
			$\eta_{vib,high}$	$\eta_{vib,mid}$	$\eta_{vib,low}$	$\eta_{vib,tot}$				
200	2.69	0.78	0.99	0.09	0.68	0.06	1.37	0.17	4.05	0.69
250	2.69	0.78	0.99	0.14	0.69	0.10	1.28	0.26	2.13	0.56
300	2.69	0.78	0.99	0.19	0.70	0.14	1.21	0.36	1.56	0.55
400	2.69	0.78	1.00	0.29	0.72	0.20	1.13	0.48	1.21	0.58
491	2.69	0.78	1.00	0.35	0.72	0.25	1.09	0.59	1.11	0.66
600	2.69	0.78	1.00	0.47	0.71	0.33	1.06	0.73	1.06	0.77
1500	2.69	0.78	1.00	0.60	0.71	0.43	1.00	0.90	1.00	0.90

[a]All calculations in this table use the MPW54/6-31+G(d,p) electronic structure level with the HR approximation for the torsion

mode.

[b]$\eta^{CVT} = \eta_{trans}\eta_{rot}\eta_{vib}\eta_{pot}$

Table VIII. Optimized geometries of the stationary points for the $H + C_2H_6$ reaction obtained from the CVBMM potential energy surface. Distances are in Å, and angles are in degrees.

	C_2H_6	Saddle point	C_2H_5
C_1-C_2	1.51	1.50	1.48
C_1-H_8	1.09	1.36	–
C_1-H_7	1.09	1.08	1.08
H_8-H_9	–	0.922	0.736
H_8-C_1-H_7	108	104	–
H_8-C_1-C_2	111	110	–
H_7-C_1-C_2	111	115	119
H_9-H_8-C_1	–	179	–

Table IX. Normal mode analysis of the stationary points of the CVBMM potential energy surface of the $H + C_2H_6$ reaction.

	Frequency (cm^{-1})			
H_2	4424			
C_2H_5	127	532	974	981
	1042	1189	1490	1498
	1503	1542	2880	2963
	2964	3056	3161	
C_2H_6	292	949	949	972
	1107	1107	1405	1464
	1464	1467	1491	1491
	2873	2963	2963	3005
	3029	3029		
Saddle Point	$1537i$	211	402	646
	848	936	962	1114
	1166	1299	1327	1379
	1397	1401	1472	1581
	2803	2884	2885	3105
	3150			

Table X. Rate constants (cm^3 molecule^{-1} s^{-1}) obtained using the CVBMM surface for the

H + C_2H_6 reaction.

T (K)	TST	CVT	CVT/SCT	Experiment
200	1.25×10^{-21}	1.24×10^{-21}	1.90×10^{-18}	n.a.
300	5.20×10^{-18}	5.20×10^{-18}	1.44×10^{-16}	n.a.
400	3.63×10^{-16}	3.63×10^{-16}	2.40×10^{-15}	n.a.
467	2.35×10^{-15}	2.35×10^{-15}	9.48×10^{-15}	1.04×10^{-14}
491	4.09×10^{-15}	4.08×10^{-15}	1.45×10^{-14}	1.42×10^{-14}
534	9.81×10^{-15}	9.80×10^{-15}	2.86×10^{-14}	2.86×10^{-14}
586	2.42×10^{-14}	2.41×10^{-14}	5.89×10^{-14}	5.45×10^{-14}
600	3.00×10^{-14}	3.00×10^{-14}	7.03×10^{-14}	n.a.
612	3.60×10^{-14}	3.59×10^{-14}	8.14×10^{-14}	7.88×10^{-14}
637	5.13×10^{-14}	5.12×10^{-14}	1.09×10^{-13}	1.08×10^{-13}
693	1.05×10^{-13}	1.04×10^{-13}	1.98×10^{-13}	2.21×10^{-13}
748	1.92×10^{-13}	1.91×10^{-13}	3.32×10^{-13}	2.59×10^{-13}
776	2.54×10^{-13}	2.53×10^{-13}	4.22×10^{-13}	4.40×10^{-13}
796	3.07×10^{-13}	3.06×10^{-13}	4.97×10^{-13}	4.45×10^{-13}
826	4.02×10^{-13}	4.00×10^{-13}	6.28×10^{-13}	5.36×10^{-13}
1000	1.45×10^{-12}	1.44×10^{-12}	1.96×10^{-12}	n.a.
1500	1.36×10^{-11}	1.35×10^{-11}	1.54×10^{-11}	n.a.
2000	4.89×10^{-11}	4.84×10^{-11}	5.20×10^{-11}	n.a.

Figure captions

Figure 1. Transition state geometry for the $H + C_2H_6 \rightarrow H_2 + C_2H_5$ reaction.

Figure 2. Rotational barrier (in cm^{-1}) of the transition state for the $H + C_2H_6 \rightarrow H_2 +$ C_2H_5 reaction at the MPW54/6-31+G(d,p) level.

Figure 3. V_a^G for the four reactions as a function of reaction coordinate s obtained using the MPW54/6-31+G(d,p) level with the HR approximation.

Figure 4. Logarithm of the deuterium KIE for reaction (R1) and (R2) vs $1000/T$ obtained using the MPW54/6-31+G(d,p) level with the HR approximation. k_1 is for $H + C_2H_6$, and k_2 is for $H + C_2D_6$.

Figure 5. Logarithm of the deuterium KIE for reaction (R1) and (R3) vs $1000/T$ obtained using the MPW54/6-31+G(d,p) level with the HR approximation. k_1 is for $H + C_2H_6$, and k_3 is for $D + C_2D_6$.

Figure 6. Logarithm of the deuterium KIE for reaction (R1) and (R4) vs $1000/T$ obtained using the MPW54/6-31+G(d,p) level with the HR approximation. k_1 is for $H + C_2H_6$, and k_4 is for $D + C_2H_6$.

Figure 7. Comparison of the plot of V_{MEP} for the $H + C_2H_6$ reaction as a function of reaction coordinate s obtained by using the CVBMM surface and the MPW54/6-

31+G(d,p) level.

Figure 8. Comparison of the plot of V_a^G for the H + C_2H_6 reaction as a function of reaction coordinate s obtained by using the CVBMM surface and the MPW54/6-31+G(d,p) level.
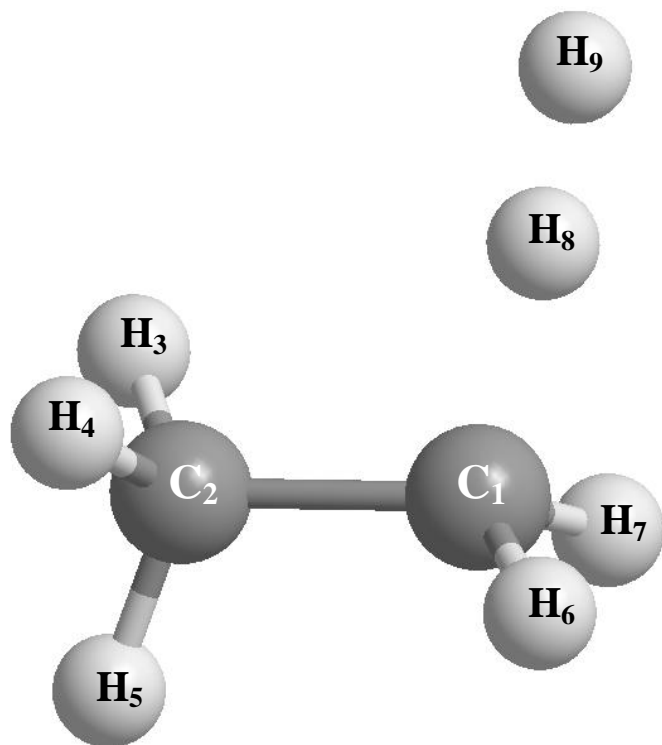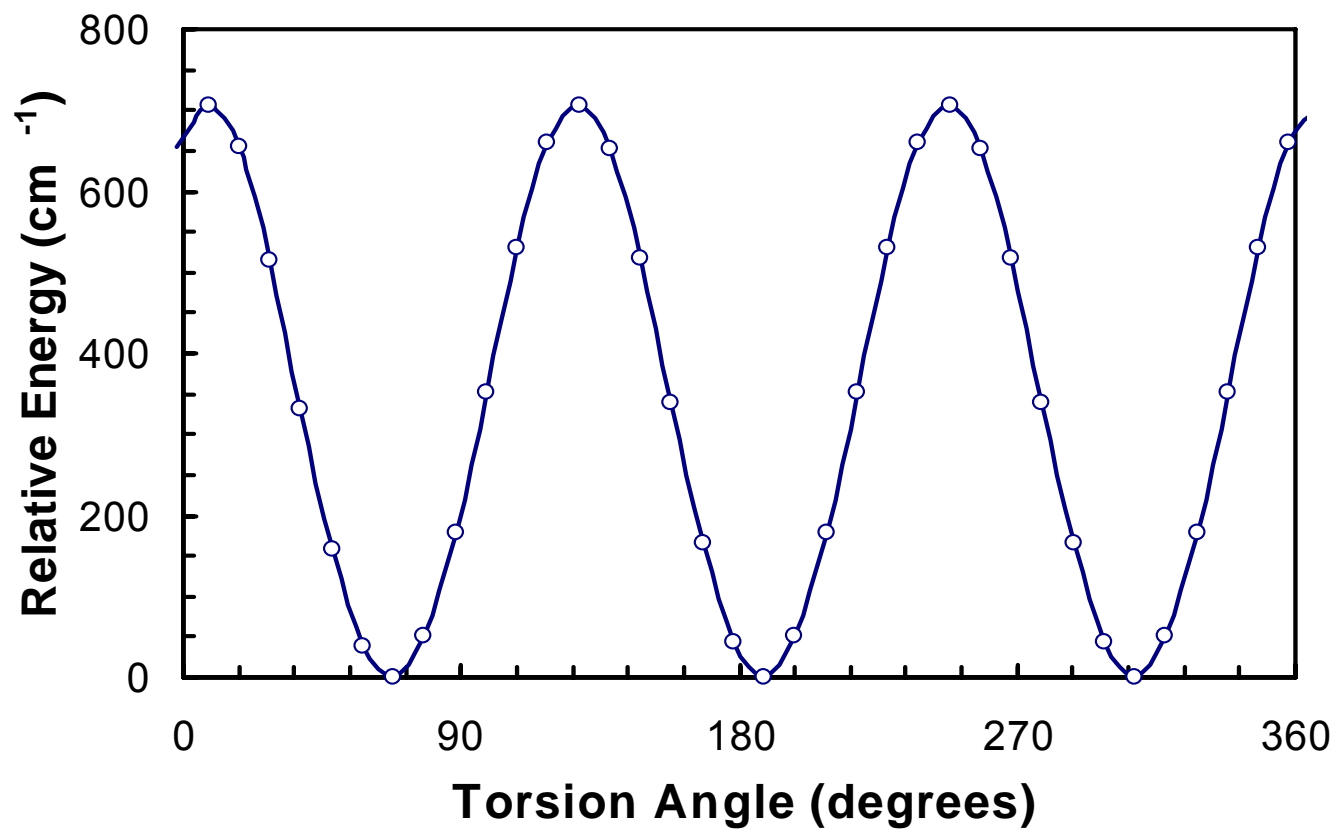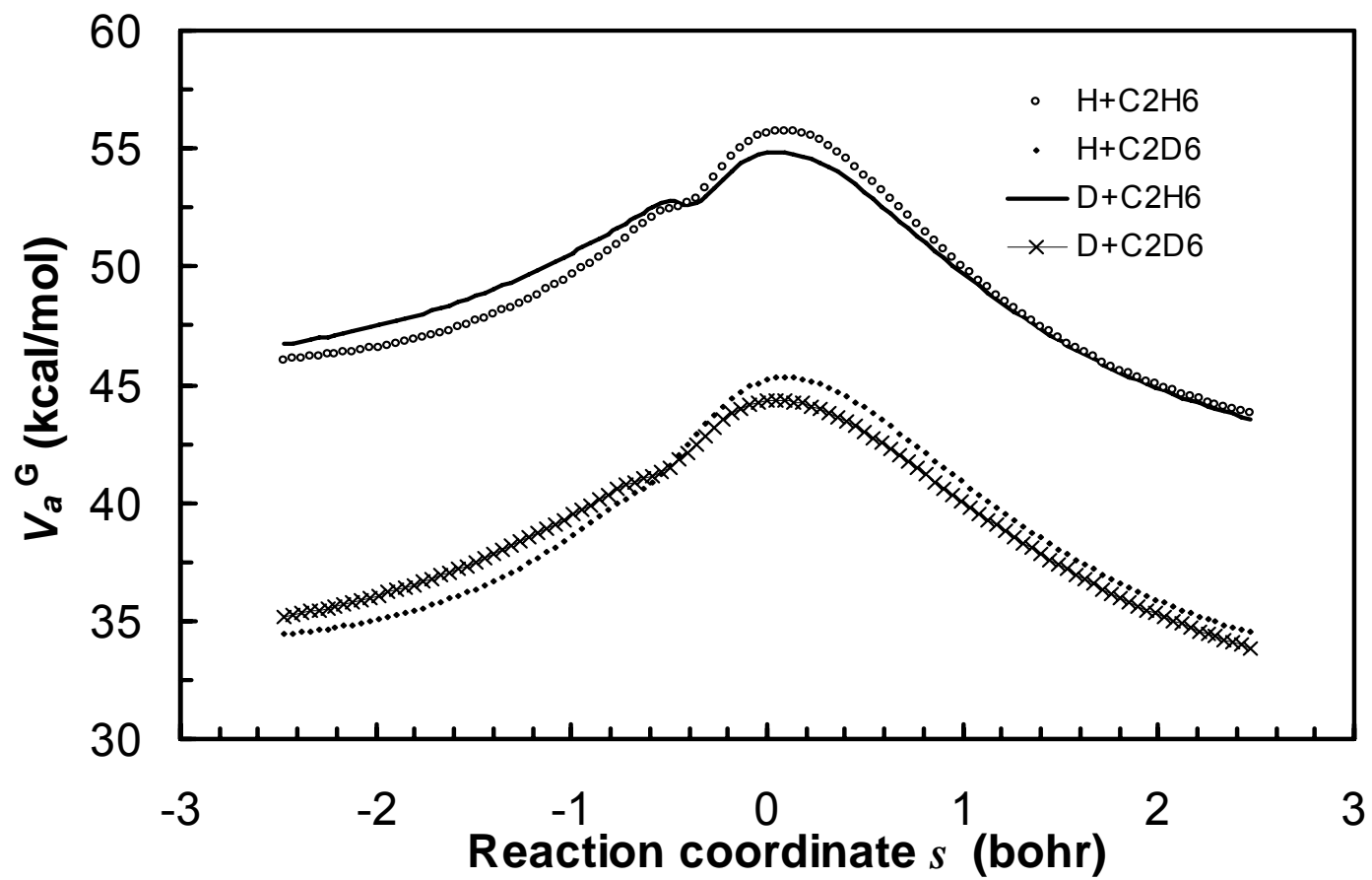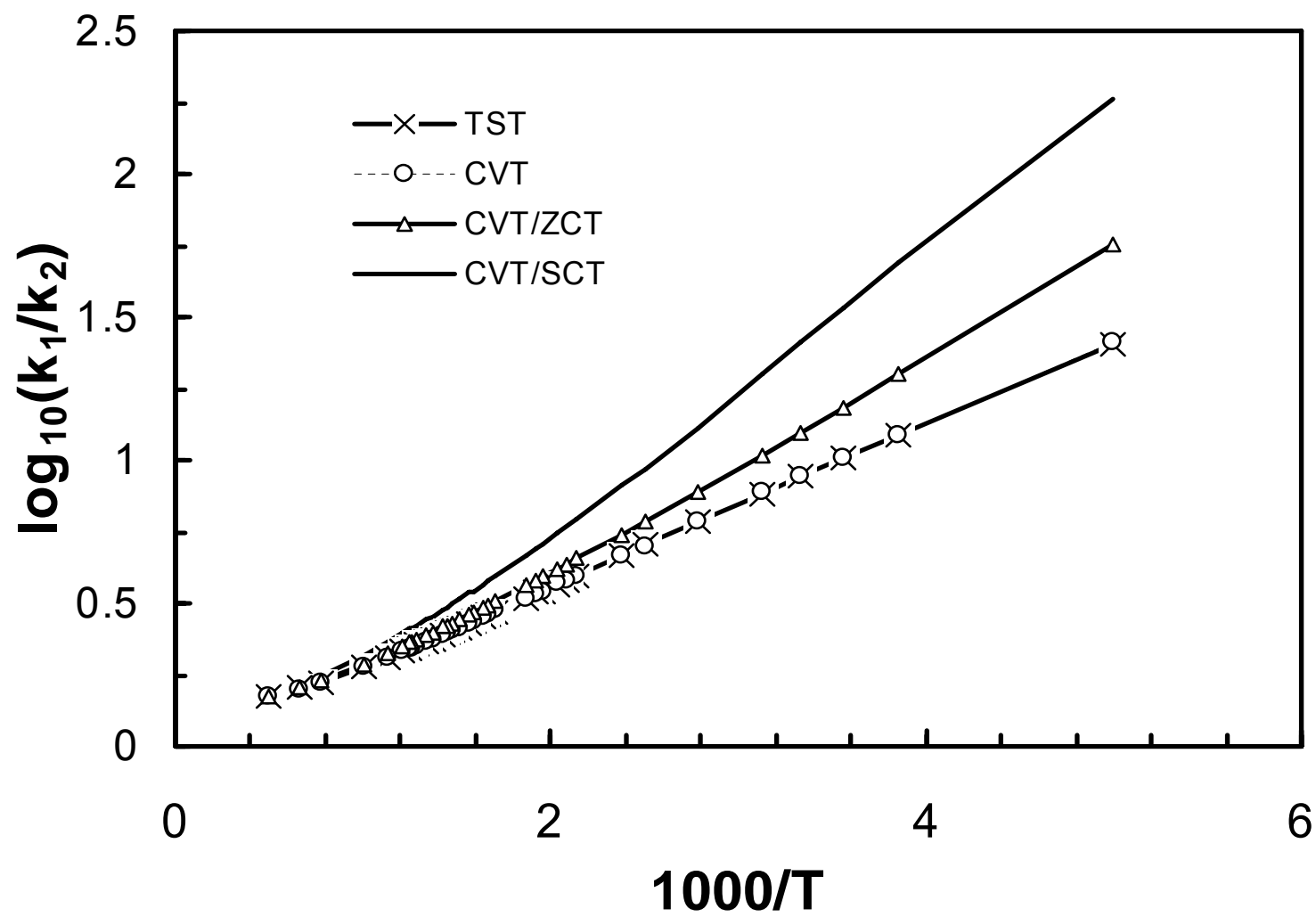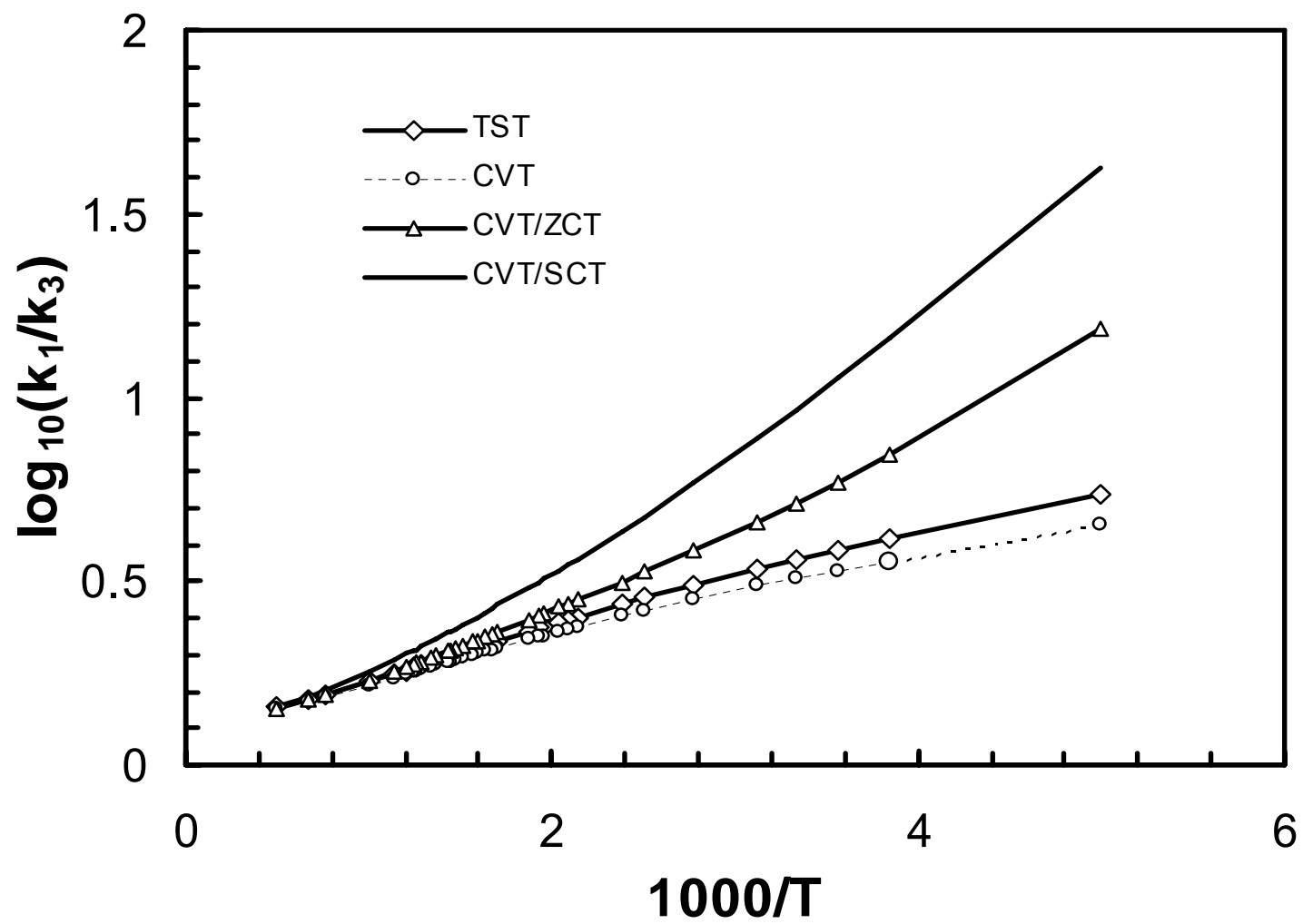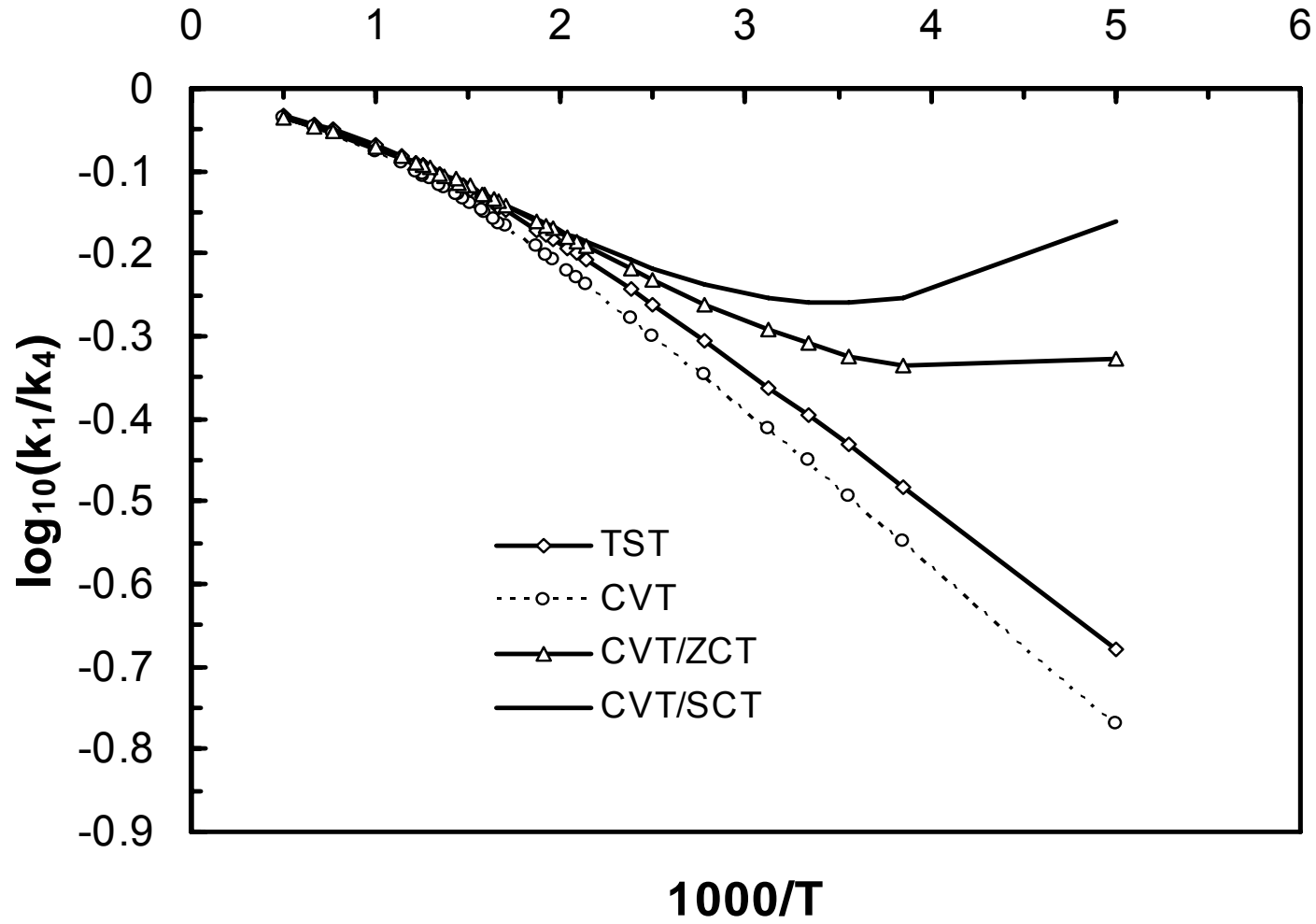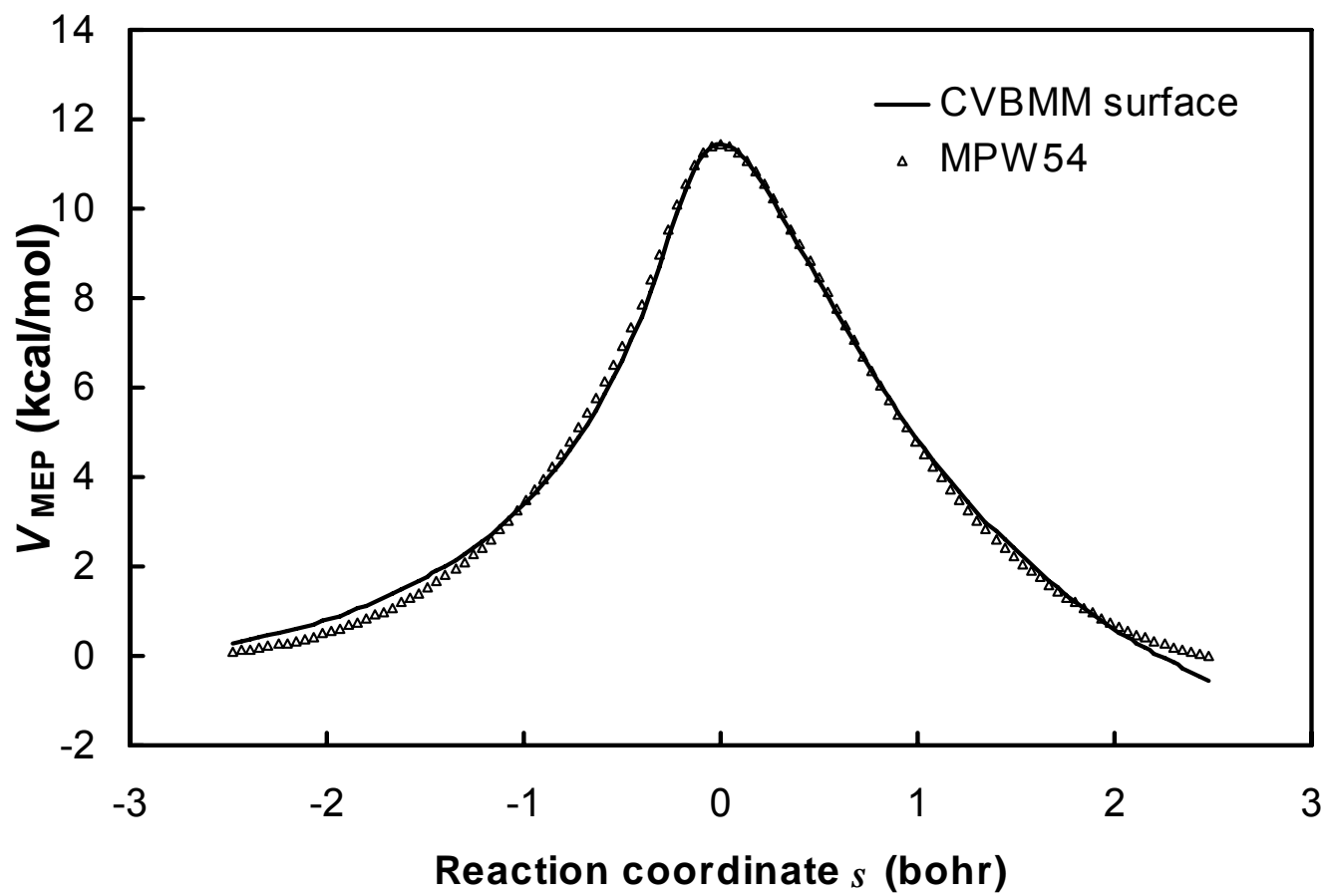
Figure 1.

Figure 2.

Figure 3.

Figure 4.

Figure 5.

Figure 6.

Figure 7.

Figure 8.